
ENERGY-EFFICIENCY LIMITS ON TRAINING AI SYSTEMS USING LEARNING-IN-MEMORY

Zihao Chen¹, Johannes Leugering², Gert Cauwenberghs², and Shantanu Chakrabartty¹

¹Department of Electrical and System Engineering, Washington University in St. Louis, St. Louis, MO, USA

²Department of Bioengineering, University of California San Diego, La Jolla, CA, USA

¹{*czihao, shantanu*}@wustl.edu

²{*jleugering, gcawwenberghs*}@ucsd.edu

ABSTRACT

Learning-in-memory (LIM) is a recently proposed paradigm to overcome fundamental memory bottlenecks in training machine learning systems. While compute-in-memory (CIM) approaches can address the so-called *memory-wall* (i.e. energy dissipated due to repeated memory *read* access) they are agnostic to the energy dissipated due to repeated memory *writes* at the precision required for training (the *update-wall*), and they don't account for the energy dissipated when transferring information between short-term and long-term memories (the *consolidation-wall*). The LIM paradigm proposes that these bottlenecks, too, can be overcome if the energy barrier of physical memories is adaptively modulated such that the dynamics of memory updates and memory consolidation match the gradient-descent dynamics when training an AI model. In this paper, we derive theoretical estimates for energy dissipated when training AI systems using different LIM approaches. The analysis presented here is model-agnostic and highlights the trade-off between energy efficiency, precision, and the speed of training. The resulting non-equilibrium energy-efficiency estimates are a function of the number of floating-point operations (FLOPs) used for training, the size of the AI model, and the precision of the training parameters. Using these results, our projections suggest that the energy required to train a brain-scale AI system (comprising of 10^{15} parameters) using LIM is in the order of $10^8 \sim 10^9$ Joules, which is 6 to 7 orders of magnitude lower than the projections obtained using energy dissipation models for state-of-the-art compute/memory systems.

Keywords AI · Training · Energy-efficiency · Landauer's limit · Learning-in-memory

Introduction

Over the past few years, the success of artificial intelligence (AI) systems has been characterized by a rapid increase in the size and complexity of the mathematical models used[1]. This growth has been driven not only by the availability of large data sets for training but also by advances in hardware accelerators capable of training these complex models within reasonable time and energy constraints. However, this rapid growth has also highlighted significant challenges in achieving the ultimate goal of developing a general or brain-scale AI system [2, 3]. The challenge is evident from the trends shown in Fig. 1, which plots the relationship between the reported number of floating-point operations (FLOPs) required to train AI systems of different sizes and the number of trainable parameters. For smaller models (with fewer than 1 billion parameters), the number of training FLOPs scales quadratically with the number of parameters. However, this trend is unsustainable for training large-scale AI models, and much effort has been devoted to finding more efficient training methods. The scaling for large language models (LLMs) appears to be linear, as depicted in Fig. 1A. Assuming that this favorable trend will continue for larger models, it can be projected

This work is supported by the National Science Foundation with research grant FET-2208770. All correspondence regarding this manuscript should be addressed to *shantanu@wustl.edu*

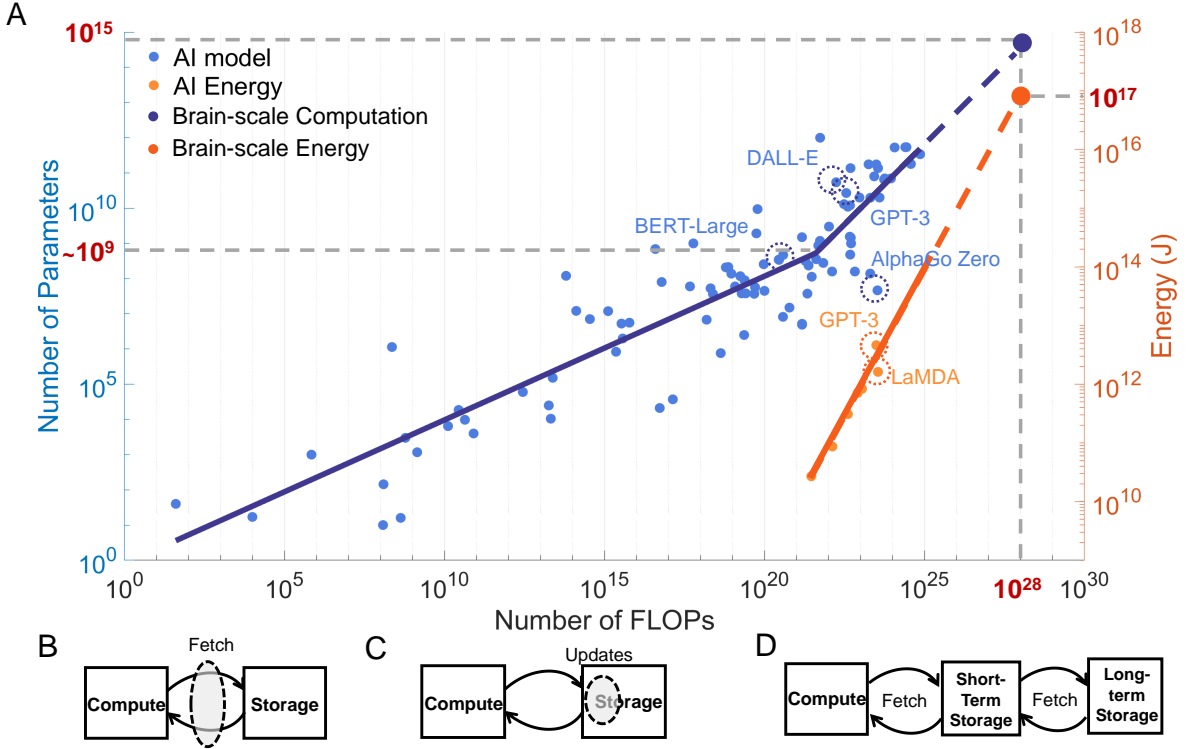


Figure 1: **Projected energy footprint for training a brain-scale AI system and associated memory bottlenecks:**(A) Trends showing the growth of computational and energy needs for training AI models [6], which has been used to predict the 10^{28} FLOPs and 10^{17} J of energy that would be needed to train a brain-scale AI model. (B) *Memory-wall* which arises due to frequent memory access by remote compute units; (C) *Update-wall* which arises due to high energy cost of memory writes at a required precision; (D) *Consolidation-wall* which arises due to limited memory capacity and hence repeated data transfers across different memory hierarchy (short-term and long-term storage).

that the number of FLOPs required to train a brain-scale AI system comprising 1 quadrillion parameters (roughly the number of synapses in a human brain [4, 5]) would be around 10^{28} , as shown in Fig. 1A.

To estimate the total energy that might be required to train such a system, we use another trend that relates the energy consumption to the number of FLOPs used during training. The trend shown in Fig. 1A appears to be linear and is benchmarked against reported energy dissipation metrics for several AI systems [7, 8, 9]. By extrapolating this FLOPs-to-energy relation to a brain-scale AI model one can estimate the energy required to train the model to be 10^{16} J or equivalently 2.78×10^6 MWh, as shown in Fig. 1A. For reference, this energy estimate equals the energy consumption of a typical U.S. household for 250,000 years [3, 10]. Such an unsustainable energy footprint for training AI systems in general, and in particular for deep-learning systems, has also been predicted in recent empirical reports and analyses [11]. Also, note that these energy dissipation estimates correspond to only a single round of training, whereas many commercial applications of large-scale AI models or their use in scientific discovery may require multiple rounds of training [12, 13, 14], further exacerbating the total energy footprint.

Similar to many other large-scale computing tasks, the energy footprint for training AI systems is determined primarily by bottlenecks due to memory access and updates [15, 16]. Training AI systems involves searching over a large set of parameters and hence requires repeated memorization, caching, and pruning. In a conventional Von-Neumann computer architecture, where the compute and memory units are physically separated from each other, frequent parameter access and updates across the physical memory hierarchy contribute to significant energy dissipation. The resulting memory bottlenecks can be categorized into three *performance walls* [17] namely: the *memory-wall*, the *update-wall*, and the *consolidation-wall*, all of which are illustrated in Fig. 1B, C and D. The *memory-wall* [16] arises because of energy dissipation due to the frequent data transfers between the computation and storage units across a memory bus (depicted in Fig. 1B. In

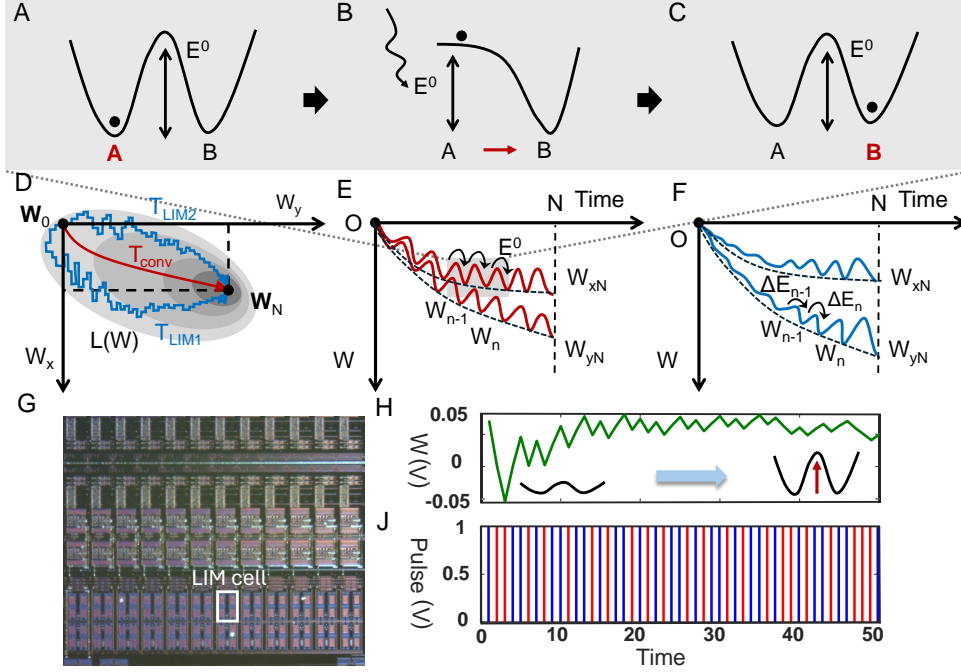


Figure 2: **Learning-in-Memory Principles:** (A) A bi-stable memory model where memory states A and B are separated by energy barrier E^0 . (B),(C) Process of state transition between consecutive memory states in a traditional analog memory. (D) A two-parameter learning model where weights W_x , W_y adapt in quantized steps to minimize a loss function $L(W)$. The red trajectory corresponds to the path resulting from deterministic mapping of the learning algorithm onto hardware memory. The blue paths correspond to possible LIM trajectories that evolve as random-walks guided by the energy gradients. (E) In a traditional memory, the transition between consecutive static states separated by constant energy barrier E^0 results in constant energy dissipation (E^0) per update. (F) Memory barrier modulation ($\Delta E_1 \dots \Delta E_n \dots$) in LIM that matches the dynamics of the learning process. (G) Micrograph of previously reported LIM cell array [29] and (H) measured results reported in [30] showing barrier modulation based on (J) external potentiation and depression pulses.

emerging AI hardware, the *memory-wall* is addressed by co-locating the memory and computation functional units [18, 19], which is in part motivated by neurobiology [20]. This compute-in-memory (CIM) paradigm has also been proposed for implementing ultra-energy-efficient neuromorphic systems [21] and analog classifiers [22] where physical synapses (memory) within the neurons (compute units) are embedded in cross-bar architectures. While the CIM paradigm can significantly improve the energy efficiency for AI inference, unfortunately, the paradigm does not address the other two performance walls due to the energy dissipation caused by memory writes (the *update-wall*), nor due to data transfers across the memory hierarchy (the *consolidation-wall*). In fact, the reliance on non-volatile memory may exacerbate these problems as the energy dissipated during memory writes is significantly higher than the energy dissipated to read the contents of a memory [23]. For AI training, both the large number of memory writes and the precision at which the memory or the parameter needs to be updated [24, 25] creates a bottleneck, hence leading to the *update-wall*, illustrated in Fig. 1C. The *consolidation-wall*, illustrated in Fig. 1D, arises due to the limited capacity of physical memory that can be integrated with or in proximity to the compute units [26, 27]. As a result, only some of the parameters of large AI models can be stored or cached locally, whereas the majority needs to be moved and consolidated off-chip. Repeated access to this off-chip memory and the consolidation overhead in maintaining a *working set* of active parameters [28] across different levels of memory cache hierarchy present a significant source of energy dissipation during AI training.

Analogous to the CIM paradigm, can neurobiology also provide cues on how to address the update- and the consolidation-walls? At a fundamental level the precision of biological synapses as storage elements is severely limited [31]. Despite this, some computations observed in neurobiology are surprisingly precise [32], which has been attributed to a combination of massive parallelism, redundancy, and stochastic encoding principles [33, 34]. In

this framework, intrinsic randomness and thermal fluctuations in the synaptic devices not only aid in achieving *higher* precision during learning but also improve the energy efficiency through noise-exploitation [35, 36]. Note that the paradigm of thermodynamics-driven (or Brownian) computing is not unique to biological synapses but has also been observed in other biological processes like DNA hybridization [37] [38] [39], and hence could be a key to address the *update-wall*. Furthermore, there is growing evidence that biological synapses are inherently complex high-dimensional dynamical systems themselves [40, 41] as opposed to the simple, static storage units that are typically assumed in neural networks. This neuromorphic viewpoint is supported by experimental evidence of *metaplasticity* observed in biological synapses [42, 43], where the synaptic plasticity (e.g. the ‘ease’ of updates) has been observed to vary depending on age and in a task-specific manner. Metaplasticity also plays a key role in neurobiological memory consolidation [44, 45], where short-term information stored in ‘volatile’, easy-to-update memory in the hippocampus is subsequently consolidated into long-term memory in the neocortex. Even though both of these spatially separated memory systems are characterized by short-term and long-term storage dynamics (similar to synthetic memory systems), they are tightly coupled to each other through distributed compute units (neurons).

Can the update- and consolidation-walls be addressed by locally adjusting the parameters of a physical memory? Recent work has demonstrated that metaplastic synapses implemented in-silico can not only be used to improve training energy-efficiency [29] but to achieve higher pattern storage capacity through memory consolidation [30]. The key premise is that if the physics of the memory elements can be exploited for parameter updates, computing, and memory consolidation, then the energy dissipated during training could be significantly reduced. Note that at the physical level, the memory elements used in most AI hardware (for e.g. static random access memory or SRAM), are static, i.e. comprise of discrete memory states (\dots, A, B, \dots) as shown using a bistable potential well [46, 47] in Fig. 2A where the states are separated from each other by fixed energy barrier E^0 . E^0 is chosen to be large enough to ensure higher memory retention and preventing memory leakage due to thermal fluctuations. For instance, in resistive random-access-memory (RRAM) devices, where the non-volatile state of the conductive filament between two electrodes determines the stored analog value [48], the energy barrier height can be as high as 1 pJ [49]. In charge-based devices like floating-gates or FeRAM, where the state of polarization determines the stored analog value [22, 50, 51], the energy barrier is typically around 10 fJ [51]. To update the memory from state $A \rightarrow B$ the energy of the state A is elevated by $\Delta E \approx E^0$ to maximize the probability of state transition to state B as shown in Fig. 2A. Note that all momentum imparted during the state transition is dissipated into the environment. In a standard AI training procedure a loss-function $L(W)$ is minimized by updating its parameter represented by a W in discrete time-steps n as ($\dots, W_{n-1}, W_n, \dots$) as shown in Fig. 2D-E. As a result the energy E^0 is dissipated for every update - irrespective of the dynamics of the optimization problem. Note that we are assuming an irreversible computing paradigm where the memory state is erased (hence the energy dissipation) before its updated with the new value (or transition to a new state). From a thermodynamic point of view, one can view this energy cost arising from the need to keep the entropy of the learning trajectories in hardware close to zero. This is illustrated in Fig. 2D using a single trajectory (denoted by the curve T_{conv}) from the initial state W_0 to the final state W_N . In practice any errors in the state update needs to be corrected by the learning algorithm which is implemented in software or in firmware.

However, if the energy barrier were modulated according to the dynamics of the learning process, i.e. where the *energy* gradient ΔE changes with the *algorithmic* gradient $\Delta L(W)$ as shown in Fig. 2F, then, like a Brownian computer [38], it is possible to thermodynamically drive both the memory update and memory consolidation processes. This principle has been the basis of the recently reported learning-in-memory (LIM) paradigm [17] where the height of the energy barrier is modulated over time in increments $\dots, \Delta E_{n-1}, \Delta E_n, \dots$ which effectively changes the update speed and the consolidation properties of the memory. Fig. 2D shows the effect of such an adaptive energy barrier modulation for a two-parameter model. Starting from an initial state W_0 surrounded by a low energy barrier, the memory updates are thermodynamically driven and guided towards the final and optimal state W_N by the loss function gradient (acting as an extrinsic field). Thus, unlike the conventional memory update dynamics, LIM dynamics exhibit a directed random-walk (or Brownian motion), as shown in Fig. 2D by trajectories $T_{LIM1,2}$, thus allowing for many possible physical paths from $W_0 \rightarrow W_N$. The principle is similar in spirit to the fungible computing paradigm [52] where multiple actions (or trajectories) could produce similar results. As the trajectories approach the optimal state towards the end of training, the memory updates become less frequent, and a higher memory retention (or low memory leakage) is required. This is achieved by increasing the height of the energy barrier as shown in Fig. 2F. The optimal barrier modulation strategy is the one that ensures that the solution to $\min_W L(W)$ is reached within an average prescribed time instant N . Here we assume that the change in the energy barrier is directly coupled to the gradient of the loss function, but in the absence of such external gradients, external energy can be injected to modulate the energy barrier of the memory leading to different variants of LIM.

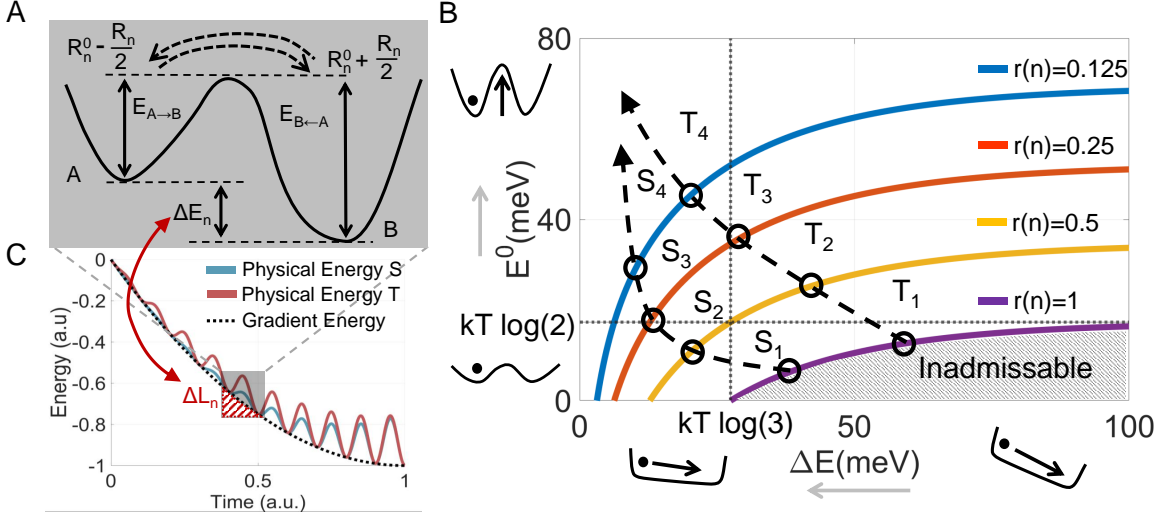


Figure 3: **The energy barrier vs energy-gradient or $(E^0 - \Delta E)$ plot** : (A) Parameters governing the thermodynamics of state transitions in a bi-stable potential well based memory model. (B) Retention (energy barrier height) versus energy gradient for different normalized update rates $r(n) = \frac{R_n}{R_{max}}$. Learning can evolve in different trajectories as the energy gradient is minimized while the retention increases, both contributing to the asymptotically decreasing update rate R . The shaded area indicates the region of inadmissible update rates. (C) Connecting physical gradient energy ΔE_n to algorithmic loss function energy ΔL_n in LIM. The height of the physical energy barriers increases at different rates which leads to different variants of LIM.

Such variants of LIM can be implemented on dynamic analog memories [29, 30] that can trade off memory retention or plasticity with the energy-efficiency of memory updates. Fig. 2G shows the micrograph of a previously reported LIM array and Fig. 2H,J shows a representative measurement result where the memory updates become less plastic (or barrier height increases) over time as write/erase pulses are applied. This *metaplastic* behavior is a signature of the barrier height modulation in LIM.

What is the estimate on energy consumption for an AI system that is trained using the LIM paradigm? - is the key question being addressed in this paper. In other words, we analyze the trade-offs between energy efficiency and speed of training for different LIM energy barrier modulation schedules. In this regard, this work differs from the adiabatic approaches that are subject to Landauer’s limit [47] and the measurement entropy limit [53, 54, 55]. These irreversible adiabatic lower bounds assume an infinite time horizon for the training to complete and, hence are impractical. However, recently these bounds have been augmented to relax the adiabatic constraints by incorporating parameters that quantify the non-equilibrium dynamics of energy transfer [56, 57]. Our exploration of the LIM-based energy-efficiency bounds is also based on a non-equilibrium approach, but our formulation establishes the connection between the energy barrier height and the hyper-parameters corresponding to the *update-* and *consolidation-wall*. To ensure that the energy estimates are agnostic to the idiosyncrasies of a learning algorithm and learning heuristics, we abstract the problem of AI training in terms of parameters that are common to all learning and optimization methods. These parameters include model size (or number of parameters stored in memory), the number of operations required to train the model, the learning-rate schedule, and the rate and precision of memory/parameter updates. The resulting formulation allows us to connect the algorithmic gradient of the loss function to the physical energy gradient and the energy barrier height using a lower bound. The lower bound can then be used to estimate the minimum energy dissipated for training AI models using different LIM variants.

Results

The first theoretical result is based on the abstract memory model using a bi-stable potential well [38, 58] shown in Fig. 3A comprising of the states A and B that are separated by an energy barrier of height E^0 which prevents state transitions $A \rightleftharpoons B$. Because we are assuming a classical (non-quantum) memory, at any instant of time n , only one of the memory states is occupied. This description of physical memory is general enough and is applicable to memory devices based on electrons stored on a capacitor, changes in

conformations in molecular memory [59], DNA hybridization states [60, 61], or micro-filaments acting as memory states in a memristor.

Relation between Barrier height, Update-rate, and Extrinsic Energy

For the bi-stable potential well shown in Figure. 3A with a barrier height E_n^0 , the transition probability between the memory states $P_n (A \rightleftharpoons B)$ at time-instant n is described by Boltzmann statistics [39, 62] as

$$P_n (A \rightleftharpoons B) = \frac{R_n^0}{R_{max}} = \exp\left(-\frac{E_n^0}{kT}\right). \quad (1)$$

where R_{max} is the maximum state-transition rate determined by the physics of memory (or maximum update-rate) and R_n^0 is the baseline transition rate under equilibrium. When the energy of the potential wells corresponding to the states A and B are shifted relative to each other at time-instant n by ΔE_n , as shown in Figure. 3A, the forward state-transition rate for $A \rightarrow B$ increases to $R_n + \frac{R_n}{2}$ and the backward state-transition rate for $A \leftarrow B$ decreases to $R_n - \frac{R_n}{2}$, respectively. Thus, the net forward transition rate or the update rate at time instant n is R_n and can be written as function of the effective energy barrier heights $E_{A \rightarrow B}$ and $E_{A \leftarrow B}$, where $E_{A \rightarrow B} = E_{A \leftarrow B} - \Delta E_n$. The relationship between the update rate R_n , gradient energy ΔE_n and the energy barrier E_n^0 is given by

$$E_n^0 = kT \log \left[\frac{2R_{max}}{R_n} \cdot \frac{\exp\left(\frac{\Delta E_n}{kT}\right) - 1}{\exp\left(\frac{\Delta E_n}{kT}\right) + 1} \right]. \quad (2)$$

and its derivation can be found in the Methods Section B.

In Fig. 3B we plot Eq. 2 for different values of the normalized update rate $R = \frac{R_n}{R_{max}}$. Along the x-axis (i.e. for $E^0 = 0$) the energy barrier is absent and the memory updates are driven directly by the presence of the external field ΔE_n . Along the y-axis (i.e. $\Delta E = 0$), the gradient is absent, hence the memory update rate is zero; however, increasing the energy barrier E^0 increases the memory retention rate. Note that in Eq. 2, for $R_n = R_{max}$ and $\Delta E \rightarrow \infty$ we recover the Landauer's limit $E_n^0 = kT \log(2)$ [47]. On the other hand, when $E_n^0 = 0$, we can achieve $R_n = R_{max}$ for $\Delta E = KT \log(3)$, which sets an upper limit on the extrinsic energy that can be injected to increase the update rate. Fig. 3B also shows the infeasible/inadmissible region where $R = \frac{R_n}{R_{max}} > 1$, i.e. where R_n exceeds the maximum update-rate R_{max} . During the process of learning, computation first proceeds at a rate R_n such that $R_{max} > R_n > 0$ (in the presence of extrinsic energy ΔE), but asymptotically, as $n \rightarrow \infty$ and the training process converges, $R_n \rightarrow 0$. At the end of the training, the learned parameters need to be retained, therefore memory leakage is reduced by increasing the height of the energy barrier. Different LIM training algorithms will follow different trajectories on the $E^0 - \Delta E$ plot, as shown by S_1, S_2, \dots and T_1, T_2, \dots in Fig. 3B. Fig. 3C and D show the corresponding energy barrier time evolution for the trajectories S and T . For trajectory S the barrier height increases quadratically with time whereas for trajectory T the barrier grows linearly. The length of the trajectory corresponds to the total training time and is determined by the loss-function $L(W)$ and its algorithmic gradient ΔL_n , as shown in Fig. 3C. Essentially, all LIM dynamics can be characterized by trajectories in the $E_n^0 - \Delta E_n$ space, and each of these trajectories would dissipate different energy based on the temporal profile of E_n^0 and ΔE_n .

Relation between Barrier height, Update-rate and Learning-rate

The LIM update dynamics is closely related to the dynamics of a learning algorithm. As shown in Fig. 3C, the algorithmic gradient ΔL_n at time instance n can be mapped to the energy gradient ΔE_n or the physical energy that drives the state transition $A \rightarrow B$. If the model parameters are updated according to a gradient-descent based rule $\Delta \mathbf{w}_n = -\epsilon_n (\mathbf{K}_n^T \nabla_{\mathbf{w}} \mathbf{L}_n)$ with $\epsilon_n \geq 0$ being the learning-rate and \mathbf{K}_n being a positive-definite matrix, then the derivation in Methods Section C and D show that the gradient energy ΔE_n and the energy barrier in Eq. 2 can be expressed in terms of ϵ_n as

$$\Delta E_n \geq \left(\frac{kT}{\delta}\right) \epsilon_n \quad (3)$$

and

$$E_n^0 \geq kT \log \left[\frac{2R_{max}}{R_n} \cdot \frac{\exp(\epsilon_n/\delta) - 1}{\exp(\epsilon_n/\delta) + 1} \right]. \quad (4)$$

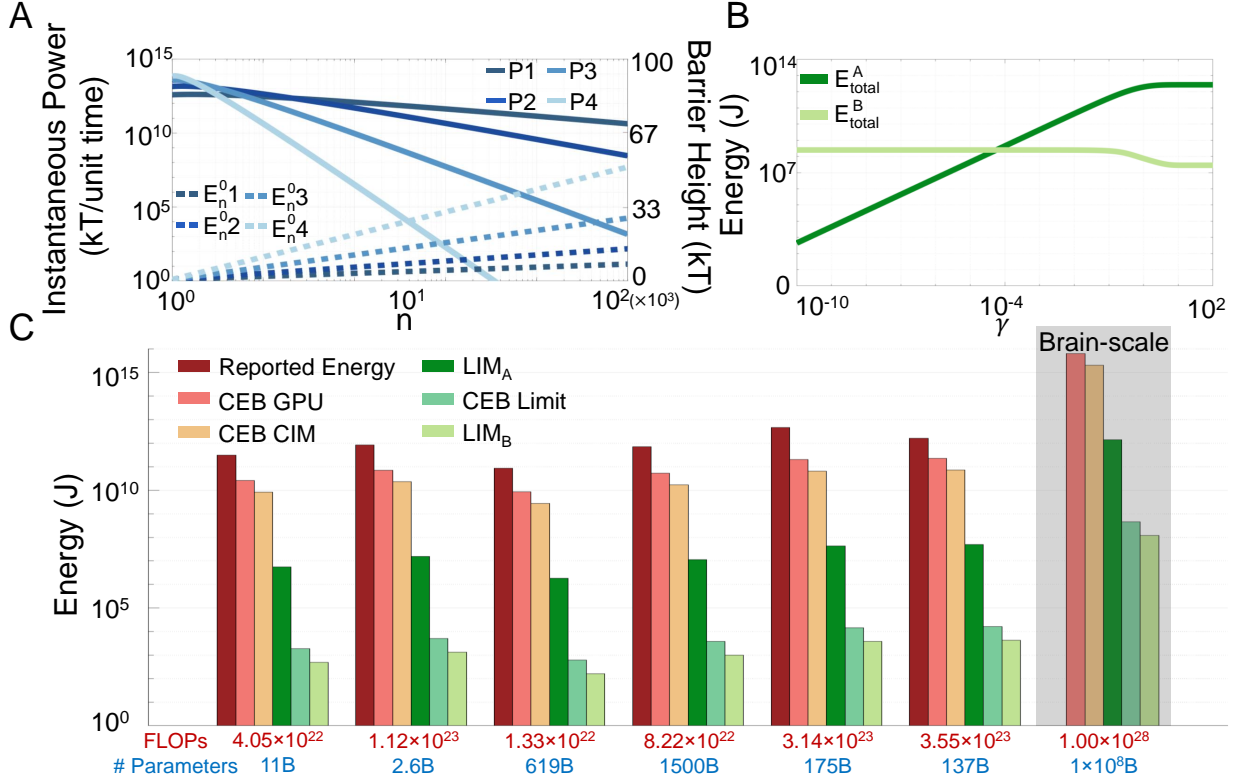


Figure 4: **Energy dissipation estimates when training using different LIM variants**(A) Estimated instantaneous power dissipation P and energy barrier height E_n^0 for training brain-scale AI using LIM_B variants with a polynomial update rate $R_n \sim \frac{1}{n^{1+\gamma}}$ with $\{P1, E_n^0 \sim \gamma = 0.5; P2, E_n^0 \sim \gamma = 2; P3, E_n^0 \sim \gamma = 5; P4, E_n^0 \sim \gamma = 10\}$; (B) Energy trade-off between LIM_A and LIM_B for different γ ; (C) Estimated energy dissipated compared against the reported energy dissipation for real-world AI training workloads [7]. From left to right, the corresponding AI models are T5, Meena, Gshard-600B, Switch Transformer, GPT-3, and LaMDA. The Brain-scale AI model estimates is for a precision $\delta = 2^{-16}$. LIM_A estimate is based on Eq. 8, LIM_B estimate is based on Eq. 32, and estimate of CEB limit is based on Eq. 9.

Here $\delta > 0$ is a hyperparameter that models the precision at which the parameters are updated and retained in memory during and at the end of training. Eq. 3- 4 are model-agnostic and connects the height of the energy barrier to the update-rate and the learning-rate. The update-rate R_n models the speed of computation at a time-instant n , and δ models the precision of the memory update/retention, both of which are metrics associated with the *update-wall*. The learning-rate ϵ_n determines the dynamics of memory-consolidation [44, 63], and hence is a metric associated with the *consolidation-wall*.

Energy dissipation estimates for LIM variants

Equations. 3- 4 show that setting two of the three parameters (learning-rate, update-rate or energy barrier-height) determines the third. This relationship can be used to estimate the total energy dissipation E_{Total} for an LIM-based training. E_{Total} is determined by the energy dissipated for building up the barrier E_∞^0 at the end of training and the energy dissipated to perform the individual state transition ΔE_n^{diss} at each time instant n . We also enforce a constraint that the total number of training operations $\#FLOPs$ is finite and is estimated from the empirical trend shown in Fig. 1A. We also constrain the update-rate schedule $r(n) = \frac{R_n}{R_{max}}$ to be monotonic $0 \leq r(\cdot) \leq 1$ such that $r(n) \rightarrow 0$ as $n \rightarrow \infty$. This choice of $r(n)$ ensures that $R_n \leq R_{max}$ and $E_n^0 \geq 0, \forall n$. Then, the lower bound of E_{Total} estimated for M memory elements can then be expressed as

$$E_{Total} \approx \#FLOPs \left[\frac{\sum_{n=1}^{\infty} \Delta E_n^{diss} r(n)}{\sum_{n=1}^{\infty} r(n)} \right] + M E_\infty^0. \quad (5)$$

The derivation of equation 5 is described in the Methods section C. Note that Eq. 5 incorporates two forms of energy dissipation: (a) the first term in Eq. 5 which represents the dynamic energy dissipated during every operation; and (b) the second term in Eq. 5 which represents the energy that is stored in the energy barriers (for memory retention). Even though the barrier energy can potentially be recycled, for our analysis we will assume that this energy cannot be recovered. Based on different energy dissipation mechanisms ΔE_n^{diss} driving the LIM updates, we can identify two variants of LIM which we will refer to as LIM_A and LIM_B respectively. For LIM_A, the memory updates are driven by the gradient energy given by Eq. 3 and shown in Fig. 3C. We show in the Methods section C that for M parameters or memory elements, the total energy dissipation E_{Total}^A for LIM_A can be estimated as

$$E_{Total}^A \approx \#FLOPs \left(\frac{kT}{\delta} \right) \left[\frac{\sum_{n=1}^{\infty} \epsilon_n r(n)}{\sum_{n=1}^{\infty} r(n)} \right] + ME_{\infty}^0. \quad (6)$$

For LIM_B, the memory updates are driven by the process shown in Fig. 2A, where external energy equal to the barrier height E_n^0 is injected to drive the memory updates. Note the barrier height changes with n , so the injected external energy also changes with n . In this case, the total energy dissipated E_{Total}^B is estimated as

$$E_{Total}^B \approx \#FLOPs \left[\frac{\sum_{n=1}^{\infty} E_n^0 r(n)}{\sum_{n=1}^{\infty} r(n)} \right] + ME_{\infty}^0. \quad (7)$$

Analytical and Numerical Estimation of Energy dissipation

Different LIM_A and LIM_B variants can be chosen based on different update-rate schedule $r(n)$ and the learning-rate schedule ϵ_n . The schedule then specifies how the barrier height should be modulated according to Eq. 4, which we use to estimate the energy dissipated E_{Total}^A and E_{Total}^B . Irrespective of the choice of gradient-descent algorithms or memory consolidation strategies, learning rate schedules are typically chosen to ensure convergence [64, 65, 66] or to maximize memory capacity [67]. This implies that $\lim_{n \rightarrow \infty} \epsilon_n = 0$ and $\sum_{n=1}^{\infty} \epsilon_n = \infty$. For example, [30, 41] propose a learning-rate schedule $\epsilon_n \approx \mathcal{O}(1/n)$, which satisfies both constraints, for achieving optimal memory consolidation. Once the learning-rate schedule is chosen to be $\epsilon_n = 1/n$, the update-rate schedule $r(n) = R_n/R_{max}$ has to decay faster than $\mathcal{O}(1/n)$ to ensure that the LIM dynamics is constrained with the feasible $E^0 - \Delta E$ plot in Fig. 3B. While several choices of $r(n)$ are possible, for the sake of exposition, we only present the results for the polynomial update-rate schedule $r(n) = 1/n^{1+\gamma}$ with $\gamma > 0$ and the Supplementary Information presents results for other update-rate schedules. For the polynomial update-rate, an analytical expression for LIM_A energy dissipation estimates can be derived from Eq. 6 as

$$E_{Total}^A \approx \#FLOPs \left(\frac{kT}{\delta} \right) \left[\frac{\zeta(2+\gamma)}{\zeta(1+\gamma)} \right] + MkT \log \left[\frac{1}{\delta} \right] \quad (8)$$

where $\zeta(\cdot)$ is the Riemann-zeta function. For LIM_B the energy dissipation estimates based on Eq. 7 cannot be obtained in closed form, hence we have to resort to a numerical approach as described in the Methods section D. However, as shown in the Methods section D the LIM_B energy dissipation estimate can be understood by focusing on two operating regimes that upper-bound and lower-bound the numerical estimate as $E_{LB}^B \leq E_{Total}^B \leq E_{UB}^B$. The analytic expression for the upper-bound estimate E_{UB}^B is based on a asymptotic operation when $\gamma \approx 0$, in which case the LIM_B energy dissipation is approximated by

$$E_{UB}^B \approx \#FLOPs \left(kT \log \left[\frac{1}{\delta} \right] \right) + MkT \log \left[\frac{1}{\delta} \right]. \quad (9)$$

Note that the expression in Eq. 9 is the same as the energy dissipation estimate for a $\log_2(1/\delta)$ bit memory/compute system with a constant energy barrier (CEB). This operation is illustrated in Fig. 2(E) and the analytical expression is derived in Methods section A. The lower-bound estimate E_{LB}^B is derived under the operating condition where $n\delta \ll 1$ and $\gamma \gg 1$ in which case the LIM_B energy dissipation is approximated by

$$E_{LB}^B \approx \#FLOPs \left(kT \log(2) - kT\gamma \left[\frac{\zeta'(1+\gamma)}{\zeta(1+\gamma)} \right] \right) + MkT \log \left[\frac{1}{\delta} \right]. \quad (10)$$

Here $\zeta'(\cdot)$ is the derivative of the Riemann-zeta function. The energy-dissipation estimates given by Eq. 8-Eq. 10 show that while for $\gamma \rightarrow 0$ LIM_A strategy is better than LIM_B, as γ increases LIM_B strategy becomes more energy efficient than LIM_A. This also highlights the different mode of operation for the two LIM variants. In fact, Eq. 9 shows that LIM_B more energy efficient than the conventional digital computing approaches with a constant energy barrier of $kT \log(1/\delta)$.

Fig. 4A plots the energy barrier-height $E_n^0 1 - E_n^0 4$ and the estimated instantaneous power $E_n^0 R_n$ for LIM_B with different update-rate schedules $P1 - P4$. Each schedule corresponds to a different value of γ in $r(n) = 1/n^{1+\gamma}$. Note that for this experiment we have used the numerical expression given by Eq. 32 for parameters #FLOPS and M that correspond to a brain-scale AI workload (extrapolated from 1A). For the polynomial update-rate, the barrier height increases logarithmically, as a result the instantaneous power dissipation for LIM_B decreases monotonically. Also note that at the end of the training E_∞^0 is higher and satisfies the constraint 28.

Fig. 4B plots the estimated energy dissipation for training a brain-scale AI system using LIM_A and LIM_B for different values of γ . Note that for LIM_B, this is equivalent to estimating the area under the curve (AUC) for different update schedules shown in Fig. 4A. As evident in the figure, there exists an energy trade-off between LIM_A and LIM_B with respect to the update rate parameter γ . As the update rate decays faster, the energy consumption for LIM_A, described in Eq. 6 increases and saturates at $\gamma \approx 10$. It is important to note that as LIM_A approaches the adiabatic operation where $\gamma \rightarrow 0$, the energy consumption diminishes to 0. On the other hand, the energy dissipation for LIM_B, as shown in Eq. 7, decreases as γ increases.

Next, we estimate the LIM energy-dissipation for realistic AI workloads based on the reported metrics (training #FLOPS and number of training parameters) as shown in Fig. 1A. For comparison, we also estimated the energy dissipation for the same workloads using reported metrics for graphical processing units (GPUs), and resistive RAM(RRAM) CIM architecture [21]. The energy estimation procedure is described in the Methods Section A. For further reference, we also include the digital energy dissipation metrics based on Eq. 9 and the measured energy dissipation reported in the literature [7]. As shown in Fig. 4C, the energy dissipation estimates for both LIM_A and LIM_B are six orders of magnitude lower than the GPU and CIM estimates. Also, LIM_A estimates are higher than the CEB limit, the LIM_B estimates are lower which can indeed be attributed to the effect of barrier modulation. For a brain-scale AI workload with 10^{28} FLOPs and 10^{15} parameters, the LIM_B energy dissipation is approximately 100 MJ. Putting this into perspective, this energy lower bound for training an entire brain-scale AI model on LIM systems would be equivalent to the energy dissipation of only $\sim 67.5 - 135$ hours usage of an NVIDIA A100 GPU[68].

Discussion

In this paper we presented the energy-dissipation estimates for LIM that are model-agnostic and depends only the training #FLOPs, the number of model parameters M , the precision of memory retention δ and a hyperparameter γ that models the decay in the update-rate schedule. In particular Eq. 4 describes how the memory energy barrier height is connected to two important parameters: (a) the parameter update rate; and (b) the learning rate, both of which determine two of the three performance walls, namely, the *update-wall* and the *consolidation-wall*. For instance, the *update-wall* is reflected in the profile of the update-rate R_n for each of the parameters, and Eq. 4 shows how a specific update-profile R_n can be achieved by modulating the barrier-profile the *learning-in-memory* paradigm. Similarly, the learning rate ϵ_n determines the *consolidation-wall*. Several adaptive synaptic models have been proposed [40, 41] that show how a specific learning-rate profile can lead to optimal information transfer rate between short-term and long-term memories. In the LIM paradigm, the mechanism by which external energy is dissipated to drive the memory/synaptic updates determines the two key variants of LIM, namely LIM_A and LIM_B. In LIM_A, like a Lyapunov system, the network or the algorithmic gradient is source of energy and determines the dynamics. In LIM_B the energy is dissipated at each step to overcome the time-varying energy barrier. As a result of this key difference there is an energy dissipation trade-off between the two variants as the update rate decreases with different decay rates (determined by hyperparameter γ). As $\gamma \rightarrow 0$, it takes more LIM updates to reach a fixed number of training #FLOPs, therefore, for LIM_A the energy dissipation per update can be pushed to zero. This is evident from Eq. 8 for $\gamma \rightarrow 0$, where $\zeta(1 + \gamma) \rightarrow \infty$. For LIM_B, the energy per update is lower bounded by the Landauer limit $kT \log(2)$ and the energy dissipation increases as $\gamma \rightarrow 0$, as evident from Eq. 10. For LIM_B, the energy dissipation decreases with an increase in γ and for brain-scale AI workload, it is more energy efficient than LIM_B and the conventional digital computing approaches. However, in LIM_B energy estimation we have ignored some practical constraints. Larger values of γ or a faster update-rate decay implies that a higher R_{max} is needed to satisfy the computational constraint 22. In practice, the maximum update rate R_{max} is determined by the maximum switching frequency (f_T) of a physical switching devices. For example, silicon-germanium heterojunction bipolar transistor [69] and an ultrafast optical switch [70] can exhibit maximum switch-rates close to 1 THz, equivalently, $R_{max} \approx 10^{12} s^{-1}$.

Irrespective of the energy dissipation mechanisms, all LIM variants are based on modulating the memory energy barrier according to Eq. 4 and Fig. 3B. Energy barrier modulation supporting the LIM paradigm could

be implemented in a variety of physical substrates using emerging memory devices. For instance, recently, we reported a dynamic memory device [29] that could also be used to modulate the memory retention profile and could be an attractive candidate to implement the LIM paradigm. However, note that to approach the fundamental energy limits of training/learning one would need to address all three performance walls. Compute-in-memory (CIM) alternatives where the computation and memory are vertically integrated in massively parallel, distributed architecture offer substantially greater computational bandwidth and energy efficiency in memristive neuromorphic cognitive computing [21] approaching the nominal energy efficiency of synaptic transmission in the human brain [71]. Resonant adiabatic switching techniques in charge-based CIM [72] further extend the energy efficiency by recycling the energy required to move charge by coupling the capacitive load to an inductive tank at resonance, providing a path towards efficiencies in cognitive computing superior to biology and, in principle, beyond the Landauer limit by overcoming the constraints of irreversible dissipative computing. It is an open question whether the learning-in-memory energy bounded by Eq. 2 could also be at least partially recovered through principles of adiabatic energy recycling.

However, for practical non-reversible architectures, the dissipation limits are determined by thermodynamic principles. As illustrated in Fig. 2D, conventional AI training hardware performance one-to-one mapping between the algorithmic updates and the updates executed on hardware. As a result, the entropy of the hardware update trajectory starting from the initial state to the final state is practically zero. The energy that is dissipated in the process (by keeping the memory barrier height higher) is to ensure that the entropy does not leak out. However, this algorithm-to-hardware mapping fails to ignore two general facts about AI training algorithms or optimization algorithms: (a) parameter updates that are guided by the optimization gradients have an inherent error-correcting capability (gradients direct the updates towards the optimal solution), hence paths can absorb fluctuations; and (b) fluctuations in parameter trajectory act as regularization in many AI training algorithms and hence has beneficial effects. The LIM paradigm essentially achieves both by exploiting the combination of thermal fluctuations and memory barrier modulation and in the process dissipating less energy.

The extrapolation of the LIM energy dissipation estimates for realistic AI workloads is based on the trends shown in Fig. 1A. The relationship between model size (number of parameters) and computation complexity (number of FLOPs) was extrapolated from numbers reported in the literature. Prior to a certain model size threshold (10^9), the computation grows polynomially w.r.t. the number of parameters while this trend becomes linear after the development of AI models surpasses the inflection point. While this work did not go in-depth to investigate the quadratic-to-linear phase transition, we can speculate several possible reasons that could be topics of future research. The first reason could be a practical limitation that arises from the model size (10^9) at the phase transition. For model size less than 10^9 , the parameters could be directly stored in the main memory and as a result, the energy cost of optimal pair-wise comparison is manageable. Beyond 10^9 parameters, external storage needs to be accessed, in which case the prohibitive energy cost dictates practical online training algorithms whose complexity grows linearly. The second reasoning for the phase-transition observed in Fig. 1A could be more fundamental. It is possible that the quadratic-to-linear transition can be explained using the Tracy-Widom distribution [73], which is the universal statistical law underlying phase-transition in complex systems, such as water freezing into ice [74], graphite transitioning into diamond [75], and metals transforming into superconductors [76]. In the phase characterized by strong coupling, the system’s energy scales quadratically with the number of components/parameters. Conversely, in the phase of weak coupling, the energy is directly related to the count of components/parameters. The training of models also seems to have followed this strong-to-weak trend, deep neural network architectures have become more modular with more distinctive functionality (for example, the multi-head attention block in Large Language Models).

While the theoretical results described in the paper suggest that the minimum energy required to train a brain-scale AI system using the LIM paradigm is ~ 6 orders of magnitude lower than the projected energy dissipation for other approaches, the article does not prescribe a specific method to approach this limit. The key assumption that was made in the derivation of LIM lower bound, is mapping of the training problem into a locally convex optimization problem which was then mapped to physical energy through Lyapunov dynamics. Since LIM memory updates are performed through the physical energy gradients that are inherent to the network, the individual LIM units need to be coupled to each other to form a flat memory system. In [30] we proposed one such LIM array based on dynamic floating-gate technology, where each memory unit updates itself to minimize the overall energy consumption rather than individual local energy. Also, if the dynamics of specific AI training algorithms can be incorporated into LIM, then the energy dissipation estimates can be lowered even further. For instance, if an L_2 -norm based regularization is used improve the generalization of AI training, the regularization process is equivalent to a leaky gradient-descent. In [30] this

synergy was exploited in dynamic floating-gate memories to improve the energy efficiency of training deep neural networks.

Methods

Energy dissipation estimates for a constant energy-barrier (CEB) model

To estimate a model-agnostic energy cost for memory updates, we assume a linear relationship between the number of training FLOPs ($\#FLOPs$) and the total energy dissipation (E_{total}). This assumption is supported by empirical evidence shown in Fig. 1. For a given bit-precision ($\#bits$), we get an estimate as

$$E_{total} \approx (\#FLOPs + M) \times \#bits \times E_{bit} \quad (11)$$

where E_{bit} is the energy dissipated per state transition of a single bit. Note that the estimate in Eq. 11 also takes into account the final energy used for storing M parameters after the training has been completed. For a practical memory $E_{bit} = kT \log(1/\delta) \approx 1 \text{ fJ}$ to 1 pJ . Training a brain-scale AI system with $M = 10^{15}$ and requiring 10^{28} FLOPs (according to Fig. 1) at a precision of 16 bit would dissipate 10^2 TJ to 10^5 TJ of energy. As shown in Fig. 4C, the energy dissipation metrics estimated using Eq. 11 matches the reported energy dissipation for current state-of-the-art AI models within a constant scaling factor.

Derivation of the E^0 - ΔE bound

In Fig. 3A, if forward/backward transition rates about the baseline rate R_n^0 are represented as $R_n^0 + \frac{R_n}{2}$ and $R_n^0 - \frac{R_n}{2}$, respectively, then the net forward transition rate or the update rate R_n can be written in terms of the effective energy barrier heights $E_{A \rightarrow B}$ and $E_{A \leftarrow B}$ according to

$$\begin{aligned} R_n^0 + \frac{R_n}{2} &= R_{max} \exp\left(-\frac{E_{A \rightarrow B}^0}{kT}\right) \\ R_n^0 - \frac{R_n}{2} &= R_{max} \exp\left(-\frac{E_{A \leftarrow B}^0}{kT}\right) \end{aligned} \quad (12)$$

where $E_{A \rightarrow B}^0 = E_{A \leftarrow B}^0 - \Delta E_n$, as shown in Fig. 3A. Combining Eq. 1 and 12 leads to the update rate R_n as

$$R_n = 2R_{max} \exp\left(-\frac{E_n^0}{kT}\right) \cdot \frac{\exp\left(\frac{\Delta E_n}{kT}\right) - 1}{\exp\left(\frac{\Delta E_n}{kT}\right) + 1}. \quad (13)$$

Note that Eq. 13 models a non-equilibrium operation where the update-rate $R_n \leq R_{max}$ changes with time-varying barrier-height E_n^0 and the extrinsic energy ΔE_n . Conversely, the energy barrier required to achieve an update-rate R_n is given by

$$E_n^0 = kT \log \left[\frac{2R_{max}}{R_n} \cdot \frac{\exp\left(\frac{\Delta E_n}{kT}\right) - 1}{\exp\left(\frac{\Delta E_n}{kT}\right) + 1} \right]. \quad (14)$$

Derivation of gradient-based LIM Lower bound

Without loss of generality, we will assume that the AI model is trained by minimizing a loss function over a set of training data. The objective here is to derive energy dissipation estimates that are agnostic to the loss function and the distribution from which the training data is drawn from. Hence, we will make some general assumptions on the nature of the loss function and the training procedure used to estimate the model parameters. In the framework of supervised learning, the training algorithm is provided with a set of feature vectors $\mathcal{T} \subset \mathcal{X} : \mathcal{T} = \{\mathbf{x}_i\}, i = 1, \dots, M$ that are drawn independently from a fixed distribution. Also provided are a set of labels or target outputs $\mathcal{O} \subset \mathcal{Y} : \mathcal{O} = \{\mathbf{y}_i\}, i = 1, \dots, M$ for each of the feature vector in the set \mathcal{X} . The training algorithm then estimates the parameters $\mathbf{w} \in \mathbb{R}^D$ of a model $f : \mathcal{X} \rightarrow \mathcal{Y}$ such that a loss-function $L : \mathcal{O} \times \mathcal{O} \rightarrow \mathbb{R}_+$ is minimized over the entire training set. If \mathbf{w}_n denotes the parameter vector at time-instant n and if $\mathbf{f}_n = \mathbf{f}(\mathcal{X}; \mathbf{w}_n) = \{\mathbf{f}(\mathbf{x}_1; \mathbf{w}_n), \mathbf{f}(\mathbf{x}_2; \mathbf{w}_n), \dots, \mathbf{f}(\mathbf{x}_T; \mathbf{w}_n)\}$ denotes the AI model function evaluated on each element of the training-set \mathcal{X} at the time-instant n , then $L_n = L(f(\mathcal{X}; \mathbf{w}_n), \mathcal{Y})$

denotes the composite loss-function that is evaluated over the entire training-set at time-instant n . Although the loss-function L is convex w.r.t f or the gradient $\nabla_f L \geq 0$, due to the non-linearity of f w.r.t \mathbf{w} , L is also non-linear w.r.t the parameters \mathbf{w} . For training, we will assume that the parameters \mathbf{w} are estimated iteratively using a gradient-descent algorithm of the form

$$\Delta \mathbf{w}_n = -\epsilon_n \mathbf{K}_n (\nabla_{\mathbf{w}} \mathbf{L}_n) \quad (15)$$

where $\Delta \mathbf{w}_n$ denotes the incremental change in the parameter vector at time-instant n and $\epsilon_n > 0$ is a time-varying learning-rate hyperparameter. $\mathbf{K}_n \in \mathbb{R}^M \times \mathbb{R}^M$ is a time-varying positive-definite matrix that makes the equation 15 general enough to incorporate second-order learning methods as well. For the special case when $\mathbf{K}_n = \mathbf{I}$, where \mathbf{I} denotes an Identity matrix, equation 15 reduces to a steepest gradient-descent method. The incremental change in the loss-function ΔL_n at time instant n can be written as

$$\Delta L_n = (\nabla_{\mathbf{w}} \mathbf{L}_n)^\top \Delta \mathbf{w}_n = -\epsilon_n (\nabla_{\mathbf{w}} \mathbf{L}_n)^\top \mathbf{K}_n (\nabla_{\mathbf{w}} \mathbf{L}_n) \quad (16)$$

The positive-definite property of \mathbf{K}_n allows us to treat ΔL_n in Eq. 16 as the *energy* of a system comprising coupled memory elements. If we can physically construct such a system, then reducing the loss of the model is equivalent to bringing the system into a lower energy state. LIM assumes that the energy released due to a gradient-step ΔL_n can be recovered or harvested which can then be used to drive the memory/parameter updates. Since \mathbf{K}_n is a $M \times M$ matrix, we will assume that the AI model comprises M physical memory elements. Thus, the algorithmic energy gradient ΔL_n can be connected to the extrinsic physical energy ΔE_n per memory element in Eq. 14 as

$$M \Delta E_n = -\beta kT \Delta L_n. \quad (17)$$

where $\beta > 0$ is a conversion factor connecting the magnitude of the algorithmic gradient step L_n to the physical energy E_n . If $\lambda_{min} > 0$ denotes the smallest eigenvalue of $\mathbf{K}_n, \forall n$, then ΔE_n in Eq. 17 can be bounded from below by

$$\Delta E_n \geq \beta \frac{kT}{M} \epsilon_n \lambda_{min} \|\nabla_{\mathbf{w}} \mathbf{L}_n\|_2 \quad (18)$$

where $\|\cdot\|_2$ denotes an L_2 norm of the vector. If we also assume that the training algorithm reaches the neighborhood of a local minimum, where the neighborhood is defined by the region around $\nabla_{\mathbf{w}} \mathbf{L}_n = \mathbf{0}$ within P bits of precision, then $\|\nabla_{\mathbf{w}} \mathbf{L}_n\|_2 \geq M 2^{-2P}$. Denoting a hyperparameter C that captures all the learning model dependent parameters according to $C = \beta \lambda_{min} 2^{-2P}$, Eq. 18 combined with Eq. 14 leads to

$$\Delta E_n \geq kTC \epsilon_n \quad (19)$$

and

$$E_n^0 \geq kT \log \left[\frac{2R_{max}}{R_n} \cdot \frac{\exp(C\epsilon_n) - 1}{\exp(C\epsilon_n) + 1} \right]. \quad (20)$$

Eq. 20 shows the connection between the height of the energy barrier to key metrics associated with the *update-wall* and the *consolidation-wall*. Both Eq. 19 and 20 model different mechanisms of energy that drives the LIM memory updates in Fig. 3B, and hence leads to two variants LIM_A and LIM_B.

Asymptotic calibration of LIM hyperparameter

Here we relate the model-specific hyperparameter C in Eq. 20 to an LIM parameter that is model agnostic. For gradient-based learning the parameter $\epsilon_n > 0$ needs to satisfy the following dynamic constraint:

$$\begin{aligned} \lim_{n \rightarrow \infty} \epsilon_n &= 0 \\ \sum_{n=1}^{\infty} \epsilon_n &= \infty. \end{aligned} \quad (21)$$

While many time-schedules for ϵ_n satisfying the constraints 21 are admissible, an $\epsilon_n = \mathcal{O}(1/n)$ schedule has been proposed [30, 41] for achieving optimal memory consolidation in benchmark random pattern experiments. For the training to terminate, the update-rate R_n should also decay asymptotically to zero which leads to the constraint

$$\lim_{n \rightarrow \infty} R_n = 0. \quad (22)$$

Again, numerous choices for scheduling R_n to satisfy the constraint 22 are possible. However, a natural choice is a polynomial decay $R_n = R_{max}/n^{1+\gamma}$ with $\gamma \geq 0$ which ensures that $E_n^0 \geq 0 \forall n$. We now use the

condition $\gamma = 0$ to determine the value of the hyper-parameter C . Note that for this condition the total number of updates becomes unbounded or

$$\sum_{n=1}^{\infty} R_n = \infty. \quad (23)$$

The asymptotic barrier height E_{∞}^0 can be estimated by inserting the respective schedules for ϵ_n and R_n in the equation 20 which leads to

$$E_{\infty}^0 \geq \lim_{n \rightarrow \infty} kT \log \left[2n \cdot \frac{\exp(C/n) - 1}{\exp(C/n) + 1} \right] = kT \log(C). \quad (24)$$

This asymptotic result is then equated to the modified Landauer's limit [38] which specifies the height of the energy-barrier $E^0 = kT \log(1/\delta)$ that is needed to ensure that a parameter could be stored/updated at a precision δ . Thus, from equation 24, $C = \frac{1}{\delta}$ which makes the bound in equation 20 model agnostic as

$$E_n^0 \geq kT \log \left[\frac{2R_{max}}{R_n} \cdot \frac{\exp(\epsilon_n/\delta) - 1}{\exp(\epsilon_n/\delta) + 1} \right]. \quad (25)$$

The bound now connects the barrier-height E_n^0 , the update-rate R_n , the learning-rate (a memory consolidation parameter) ϵ_n , and the precision of computation/memory retention δ .

LIM energy estimates for large AI models

For M parameters or memory elements, the total energy dissipation E_{Total} is lower bounded by

$$E_{Total} \approx M \left(kT \sum_{n=1}^{\infty} R_n \Delta E_n^{diss} \Delta t + E_{\infty}^0 \right). \quad (26)$$

where Δt denotes the duration of each discrete time step and ΔE_n^{diss} is the energy dissipated for each LIM update. In addition to the asymptotic constraints given by equations 21 and 22, we also enforce constraints to ensure: (a) termination of training within a finite number of training operations; and (b) the required memory retention at the end of training. These are specified as:

$$M \sum_{n=1}^{\infty} R_n \Delta t = \#FLOPs \quad (27)$$

$$E_{\infty}^0 \geq kT \log \left[\frac{1}{\delta} \right] \quad (28)$$

If the update-rate schedule $r(n) = \frac{R_n}{R_{max}}$ is chosen according to a monotonic function $0 \leq r(\cdot) \leq 1$, then equations 6 and 27 can be used to eliminate intermediate variables R_{max} and Δt to produce

$$E_{Total} \approx \#FLOPs \left[\frac{\sum_{n=1}^{\infty} \Delta E_n^{diss} r(n)}{\sum_{n=1}^{\infty} r(n)} \right] + ME_{\infty}^0. \quad (29)$$

For a learning rate schedule $\epsilon_n = 1/n$, the update-rate schedule $\frac{R_n}{R_{max}} = 1/n^{1+\gamma}$ with $\gamma > 0$ ensures that Eq. 27 is satisfied. In LIM_A , the energy to drive the memory updates are derived from the algorithmic gradient. Therefore, according to Eq. 19 and the asymptotic calibration, $\Delta E_n^{diss} = \epsilon_n (kT/\delta)$, Eq. 29 leads to

$$\begin{aligned} E_{Total}^A &\approx \#FLOPs \left[\left(\frac{kT}{\delta} \right) \frac{\sum_{n=1}^{\infty} \epsilon_n r(n)}{\sum_{n=1}^{\infty} r(n)} \right] + ME_{\infty}^0 \\ &= \#FLOPs \left(\frac{kT}{\delta} \right) \left[\frac{\sum_{n=1}^{\infty} \frac{1}{n^{2+\gamma}}}{\sum_{n=1}^{\infty} \frac{1}{n^{1+\gamma}}} \right] + ME_{\infty}^0. \end{aligned} \quad (30)$$

Eq. 31 can now expressed in an analytic form

$$E_{Total}^A \approx \#FLOPs \left(\frac{kT}{\delta} \right) \left[\frac{\zeta(2+\gamma)}{\zeta(1+\gamma)} \right] + MkT \log \left[\frac{1}{\delta} \right]$$

where $\zeta(\cdot)$ denotes the Riemann-zeta function.

Similarly, the energy dissipation lower bound for LIM_B can be estimated as

$$\begin{aligned}
E_{Total}^B &\approx M \left(\sum_{n=1}^{\infty} R_n E_n^0 \Delta t + E_{\infty}^0 \right) \\
&\approx MkT \Delta t \sum_{n=1}^{\infty} \frac{R_{max}}{n^{1+\gamma}} \log \left[2n^{1+\gamma} \cdot \frac{\exp(1/n\delta) - 1}{\exp(1/n\delta) + 1} \right] \\
&\quad + MkT \log \left[\frac{1}{\delta} \right]
\end{aligned} \tag{31}$$

which after using Eq. 27 leads to

$$E_{Total}^B \approx \#FLOPs \left[kT \frac{\left(\sum_{n=1}^{\infty} \frac{1}{n^{1+\gamma}} \log \left[2n^{1+\gamma} \cdot \frac{\exp(1/n\delta) - 1}{\exp(1/n\delta) + 1} \right] \right)}{\left(\sum_{n=1}^{\infty} \frac{1}{n^{1+\gamma}} \right)} \right] + MkT \log \left[\frac{1}{\delta} \right]. \tag{32}$$

For the asymptotic operation $\gamma \approx 0$ and noting that $\log \left[2n \cdot \frac{\exp(1/n\delta) - 1}{\exp(1/n\delta) + 1} \right] \leq \log \left[\frac{1}{\delta} \right], \forall n \geq 1$, the expression in Eq. 32 can be simplified as

$$E_{UB}^B \approx \#FLOPs \left(kT \log \left[\frac{1}{\delta} \right] \right) + MkT \log \left[\frac{1}{\delta} \right]. \tag{33}$$

For the case when the updates are performed at high-precision or $n\delta \ll 1$ and $\gamma \gg 1$, Eq. 32 can be simplified as

$$E_{LB}^B \approx \#FLOPs \left(kT \log(2) + kT(1 + \gamma) \left[\frac{\sum_{n=1}^N \log(n)/n^{1+\gamma}}{\left(\sum_{n=1}^{\infty} \frac{1}{n^{1+\gamma}} \right)} \right] \right) + MkT \log \left[\frac{1}{\delta} \right] \tag{34}$$

For large N , the expression in Eq. 34 can be simplified using the power series expansion of the Riemann-zeta function $\zeta(\cdot)$ and its derivative $\zeta'(\cdot)$ to obtain a closed form expression

$$E_{LB}^B \approx \#FLOPs \left(kT \log(2) - kT\gamma \left[\frac{\zeta'(1 + \gamma)}{\zeta(1 + \gamma)} \right] \right) + MkT \log \left[\frac{1}{\delta} \right]. \tag{35}$$

Supplemental Materials: Energy-efficiency Limits on Training AI Systems using Learning-in-Memory

S1.1 Energy estimation based on Landauer's Limit and measurement Limit

AI training based on a gradient-descent approach comprises two key processes: (a) for a given set of parameters (stored in memory) computing the gradients; and (b) based on the gradient-descent algorithm of choice, updating the parameters in memory. If we assume that the cost of gradient computation is zero, then the two processes can be abstracted as changing the state of the memory and measuring the current state of the memory. Since the focus of this paper is on irreversible computing, the state of the memory is changed by erasing the previously stored state and updating it with a new state based on the gradient. The thermodynamic energy dissipation for this process is bounded from below by the *Landauer limit*. This is shown in Figure S1A, where initially only the state A is occupied. As the energy barrier E^0 is lowered, both A and B states become equally likely to be occupied. The resulting erasure of the previously stored information and the resulting increase in entropy of dissipates energy E_{Landauer} given by

$$E_{\text{Landauer}} \geq kT \log 2 \approx 0.69kT. \quad (36)$$

As shown in Fig. S1A, in the state of erasure, an application of an external force (or field) can push the state towards B , after which point the energy barrier is restored to lock in the new memory state. Note that in the classical Landauer's limit, this (slow) state transition from $A \rightarrow B$ does not dissipate any additional energy because of adiabatic assumptions. Also, it is assumed that the energy injected to lower the energy-barrier E^0 can be perfectly recovered to restore the barrier, as shown in the fourth stage of Figure S1A [77]. However, this is a highly idealized assumption; in practice, some of this energy is dissipated. A lower limit on this energy is determined by the height of the energy barrier which in turn is dependent on a measurement process. Therefore, for AI training, Landauer's Limit is incomplete, since the state of the memory (parameter) needs to be read out (or measured) for computing gradients which in turn determine the next memory (or parameter) update. The measurement process is limited by thermal noise and hence the estimate of energy dissipation needs to be taken into account [54, 55].

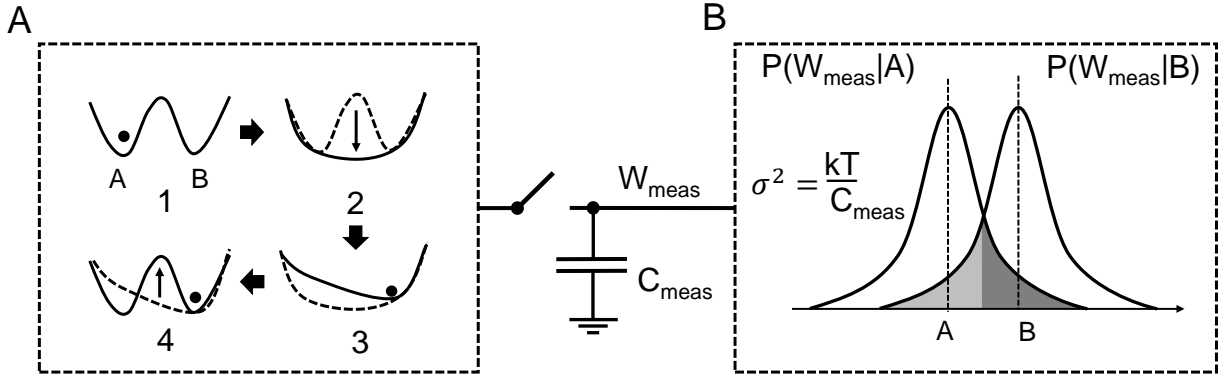


Figure S1: (A) Adiabatic process of updating the state of a bi-stable memory from state A to B which leads to the Landauer limit; (B) Measurement of the current memory state as voltages sampled on a sampling capacitor C_{meas} , which is limited by the Johnson-Nyquist thermal noise variance given by $\frac{kT}{C_{\text{meas}}}$.

As shown in Figure S1, measuring the state of the memory A or B requires sampling the stored information on a measurement capacitance C_{meas} . The measured signal W_{meas} then admits two conditional probability distributions shown as shown in Figure S1B where the variance of the Gaussian distributions $\sigma^2 = \frac{kT}{C_{\text{meas}}}$ are determined by the Johnson-Nyquist Thermal Noise [78].

Following an approach similar to what was presented in [54], we estimate the energy dissipated during the process of logic transition when the measurement capacitance C_{meas} charges and discharges to voltage W_{meas} at a clock rate of f_c , which is given by

$$P = f_c \times \frac{1}{2} C_{\text{meas}} W_{\text{meas}}^2. \quad (37)$$

Moreover, the energy dissipated per bit is then given by

$$E_{meas} = \frac{P}{C}. \quad (38)$$

where C denotes the channel capacity from Shannon's Theorem. Moreover, since we are looking for the lower bound on energy, the lower limit is obtained when the information transfer rate is adiabatic, corresponding to Figure S1A, where $p_{avg} \rightarrow 0.5$. When operating near the average probability of error $p_{avg} = p \approx 0.5$, we derive the energy it takes to perform a bit operation. The Shannon capacity equation states

$$C(p) = f_c[1 + p \log_2 p + (1 - p) \log_2 (1 - p)]. \quad (39)$$

Defining Δp as $\Delta p = p_{avg} - 0.5$ and using a Taylor series expansion of $C(p)$ around $p_{avg} = p = 0.5$, equation 39 leads to,

$$\begin{aligned} C(\Delta p)|_{p \approx 0.5} &= C(p) + \frac{C'(p)}{1!} \Delta p + \frac{C''(p)}{2!} \Delta p^2 + \dots \\ &= \frac{2}{\ln 2} f_c (\Delta p)^2 \end{aligned} \quad (40)$$

Assuming that the variance of measurement $\sigma^2 = \sigma_1^2 = \frac{kT}{C_{meas}}$ as determined by thermal-noise and $V_{th} = \frac{W_{meas}}{2}$, Δp is given by

$$\Delta p \approx \frac{g(0)W_{meas}}{2} = \frac{W_{meas}}{2\sqrt{2\pi}\sigma} = \frac{W_{meas}}{2\sqrt{2\pi kT/C_{meas}}} \quad (41)$$

where $g(\cdot)$ is the Gaussian distribution function. Using Eq. 40, the capacity is given by

$$C_{MBL}|_{p \approx 0.5} = \frac{W_{meas}^2}{(4\pi \ln 2) \frac{kT}{C_{meas}}} f_c \quad (42)$$

which leads to the fundamental energy limit as

$$E_{meas} = \frac{P}{C(p)|_{p \approx 0.5}} \approx 4.35kT/bit. \quad (43)$$

Therefore, combining Landauer's limit with the measurement limit leads to the adiabatic energy-dissipation limit per bit of operation as

$$E_{Lim} = 4.35kT/bit + 0.69kT/bit = 5.04kT/bit. \quad (44)$$

For a bit-precision ($\#bits$), Eq. 44 can be used to estimate the total energy dissipation based on the Landauer and measurement limits as

$$E_{total}^{Lim} \approx (\#FLOPs + M) \times \#bits \times E_{Lim}. \quad (45)$$

Here the $\#FLOPs$ denotes the number of compute operations required for training the AI model with M parameters. Note that Eq. 45 is a special form of constant energy barrier (CEB) estimation approach with

$$E_{total}^{Lim} \approx (\#FLOPs + M) \times kT \log \left[\frac{1}{\delta} \right] \quad (46)$$

where $\delta = 2^{-\log_2 e \times 5.02 \times \#bits}$ is the precision for each compute step and memory retention at the end of training. Note that the estimate E_{total}^{Lim} accounts for the thermal fluctuations during the process of memory state transfer onto the measurement capacitance at the adiabatic limit, as well as the entropy gain due to the computation. But it relies on thermal equilibrium dynamics to perform the memory state transition, which implies an adiabatic (i.e. slow) information transfer rate, and thus severely underestimates the power consumption of any real-world applications that require non-equilibrium dynamics to sustain a higher information transfer rate.

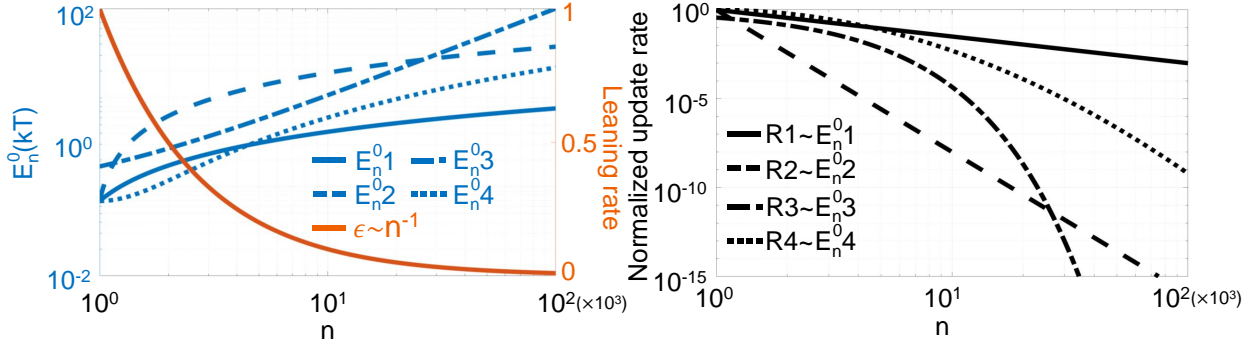


Figure S2: Update rates $\frac{R_n}{R_{max}}$, $R1 - R4$ for (A) different energy barrier E_n^0 schedules and for an optimal consolidation rate schedule $\epsilon_n \sim 1/n$ where : (B) $\{R1 \sim n^{-1.5}, R2 \sim n^{-8}, R3 \sim e^{-n}, R4 \sim n^{-\log n}\}$

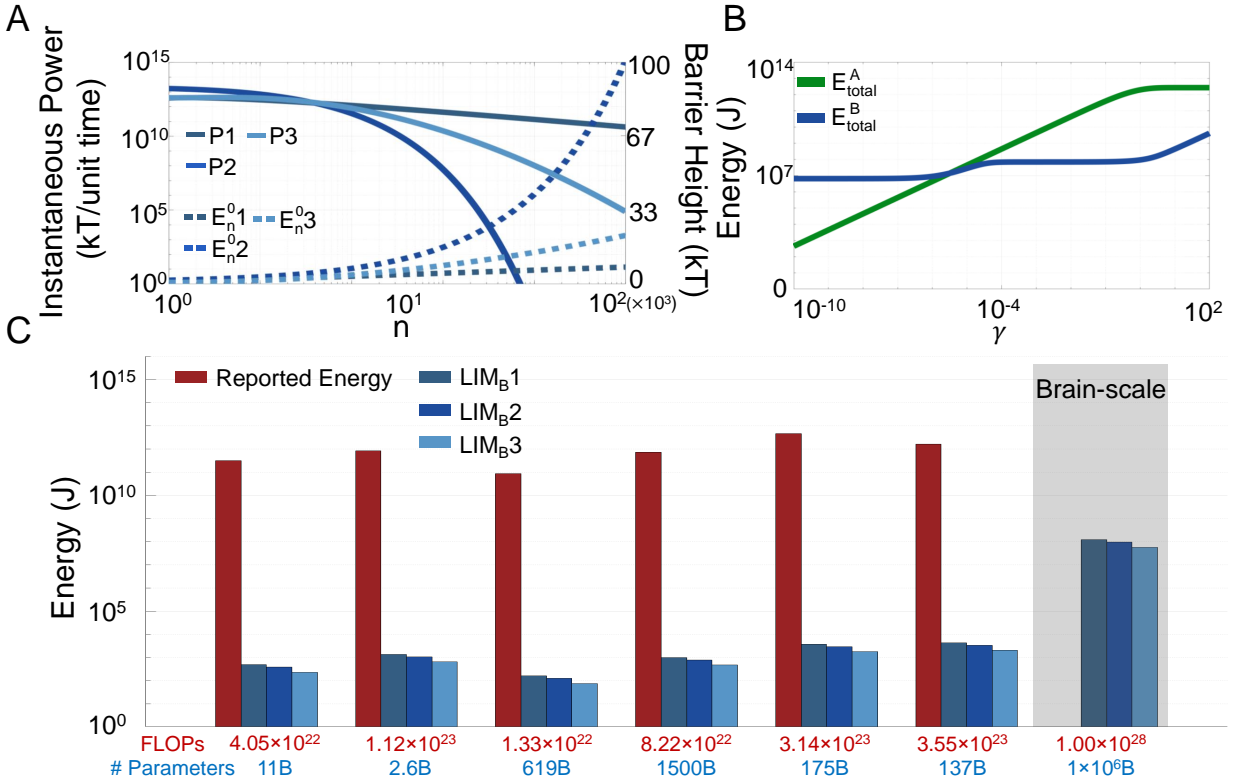


Figure S3: **Energy dissipation estimates when training using different LIM variants under various update schedules**(A) Estimated instantaneous power dissipation P and energy barrier height E_n^0 for training brain-scale AI using LIM_B variants with different update rates with $\{P1, E_n^0$ 1 $\sim \frac{1}{n^{1.5}}$; $P2, E_n^0$ 2 $\sim e^{-n}$; $P3, E_n^0$ 3 $\sim n^{-\log n}\}$; (B) Energy trade-off between LIM_A and LIM_B for different γ in exponentially decaying update rate $r(n) \sim e^{-\gamma n}$ as derived in Section S1.3; (C) Estimated energy dissipated for different LIM_B schedules compared against the reported energy dissipation for real-world AI training workloads. The Brain-scale AI model estimates are for a precision $\delta = 2^{-16}$.

S1.2 Numerical Simulation of Different Update Rate Schedules

In this set of experiments, we achieve the desired update rate R_n dynamics by controlling the dynamics of E_n^0 under fixed consolidation rate schedule $\epsilon_n \sim 1/n$. Figure S2 shows several examples of update schedules that can be realized by changing the barrier height E_n^0 with respect to discrete unit time n which is depicted along the x-axis. The time evolution of E_n^0 is chosen to obtain the predetermined update dynamics such that it satisfies the constraints on the update rate R_n .

The learning rate schedule $\epsilon_n \sim 1/n$ is chosen for optimal memory consolidation [79] [80] which is achieved under specific operating conditions. Figure S2B plots the update-rate R_n resulting from the choice of ϵ_n and E_n^0 dynamics. The trade-offs among the different schedules are evident in Figure S2A and (b), where faster-increasing energy barrier E_n^0 incurs faster decaying update rate R . As a result, the final energy-barrier E_N^0 is higher when the training stops, thus satisfying constraint on the magnitude of the energy barrier E_N^0 , which ensures that the learned parameters are retained. However, when R_n decays faster with time, R_{max} needs to be chosen to be higher to ensure that the computational constraints on R_n is satisfied. On the contrary, for E_n^0 and corresponding R , the memory retention is poor but the required R_{max} is smaller. In practice, the maximum update rate R_{max} can be estimated by f_T or the maximum switching frequency of physical switching devices. For example, silicon-germanium heterojunction bipolar transistor [69] and an ultrafast optical switch [70] can exhibit maximum switch-rates close to 1 THz, equivalently, $R_{max} \approx 10^{12}/s$. Therefore, there exists a trade-off between the memory retention requirement (E_N^0) and hardware realizability (R_{max}).

S1.3 LIM analysis for exponential decay update-rate

In this section, we derive the analytical energy-dissipation estimates for LIM_A and LIM_B with exponentially-decaying update rate schedule $r(n) \sim e^{-\gamma n}$. Similar to what has been shown for a polynomial decay update-rate in the main text,

$$\begin{aligned}
E_{Total}^A &\approx M \left(\frac{kT}{\delta} \sum_{n=1}^{\infty} R_n \epsilon_n \Delta t + E_{\infty}^0 \right) \\
&= \#FLOPs \left(\frac{kT}{\delta} \right) \left[\frac{\sum_{n=1}^{\infty} \frac{1}{n} e^{-\gamma n}}{\sum_{n=1}^{\infty} e^{-\gamma n}} \right] + M E_{\infty}^0 \\
&\approx \#FLOPs \left(\frac{kT}{\delta} \right) \left[(1 - e^{-\gamma}) \log(1 - e^{-\gamma}) \right] + M kT \log \left[\frac{1}{\delta} \right]
\end{aligned} \tag{47}$$

Similarly, the energy dissipation for LIM_B can be estimated as

$$\begin{aligned}
E_{Total}^B &\approx M \left(\sum_{n=1}^{\infty} R_n E_n^0 \Delta t + E_{\infty}^0 \right) \\
&\approx M kT \Delta t \sum_{n=1}^{\infty} \frac{R_{max}}{e^{\gamma n}} \log \left[2e^{\gamma n} \cdot \frac{\exp(1/n\delta) - 1}{\exp(1/n\delta) + 1} \right] + M kT \log \left[\frac{1}{\delta} \right] \\
&= \#FLOPs \left[kT \frac{\left(\sum_{n=1}^{\infty} e^{-\gamma n} \log \left[2e^{\gamma n} \cdot \frac{\exp(1/n\delta) - 1}{\exp(1/n\delta) + 1} \right] \right)}{\left(\sum_{n=1}^{\infty} e^{-\gamma n} \right)} \right] + M kT \log \left[\frac{1}{\delta} \right]
\end{aligned} \tag{48}$$

For the purpose of obtaining a closed-form estimation of LIM_B energy dissipation, since $e^{\gamma n}$ grows much faster than $\left[\frac{\exp(1/n\delta) - 1}{\exp(1/n\delta) + 1} \right]$ as $n \rightarrow \infty$, E_{Total}^B can be estimated as

$$\begin{aligned}
E_{Total}^B &\approx \#FLOPs \left[kT \log 2 + kT \gamma \frac{\sum_{n=1}^{\infty} n e^{-\gamma n}}{\sum_{n=1}^{\infty} e^{-\gamma n}} \right] + M kT \log \left[\frac{1}{\delta} \right] \\
&\approx \#FLOPs \left[kT \log 2 + \frac{kT \gamma}{1 - e^{-\gamma}} \right] + M kT \log \left[\frac{1}{\delta} \right].
\end{aligned} \tag{49}$$

S1.4 LIM energy dissipation for different update-rate schedules

This section presents the power dissipation for different LIM rate schedules to demonstrate the trade-off between different LIM dynamics. Fig. S3A plots the energy barrier-height $E_n^0 1 - E_n^0 3$ and the estimated instantaneous power $E_n^0 R_n$ for LIM_B with different update-rate schedules P1 – P3, as shown in the caption of the figure.

Similar to what was presented in the main paper, the energy trade-off for training a brain-scale AI system between LIM_A and LIM_B is plotted in Fig. S3B. Following the derivation in Section S1.3, the total energy dissipation in this figure corresponds to exponentially decaying update rate schedule $e^{-\gamma n}$ with various values of γ . Different from the polynomially decaying dynamics as shown in the main paper, for the exponentially decaying update rates both LIM_A and LIM_B increases as the rate parameter γ increases. As shown in the figure, the energy dissipation for LIM_A saturates at $\gamma \approx 10$, while the energy for LIM_B increases linearly. This dynamics can be explained from the analytical closed-form energy dissipation as presented in Section S1.3. Note that for this experiment we have used the numerical expression given by Eq. 47 and Eq. 48 for parameters #FLOPS and M that correspond to a brain-scale AI workload as extrapolated from Fig.1A in the main texts.

Next, we estimate the LIM_B energy-dissipation under different update rate schedules for realistic AI workloads based on the reported metrics (training #FLOPS and number of training parameters), similar to Fig.4C in the main text. The energy dissipation for LIM_B1 – 3 follows a descending order, while the corresponding update rates of LIM_B2 decays faster than LIM_B3 and faster than LIM_B1. The energy dissipation of the asymptotically faster e^{-n} schedule is greater than the slower $n^{-\log n}$ schedule. This can be explained by the temporal relationship between $r(n)$ and E_n^0 and the fact that the majority of power is dissipated during the beginning phase of the training process, as shown in Fig. S3A.

References

- [1] Alec Radford, Jeffrey Wu, Rewon Child, David Luan, Dario Amodei, Ilya Sutskever, et al. Language models are unsupervised multitask learners. *OpenAI blog*, 1(8):9, 2019.
- [2] Hans Moravec. When will computer hardware match the human brain. *Journal of evolution and technology*, 1(1):10, 1998.
- [3] Alex de Vries. The growing energy footprint of artificial intelligence. *Joule*, 7(10):2191–2194, 2023.
- [4] Suzana Herculano-Houzel. The human brain in numbers: a linearly scaled-up primate brain. *Frontiers in Human Neuroscience*, 3, 2009.
- [5] Suzana Herculano-Houzel. *Neuronal scaling rules for primate brains*, page 325–340. Elsevier, 2012.
- [6] Charlie Giattino, Edouard Mathieu, Veronika Samborska, and Max Roser. Artificial intelligence. *Our World in Data*, 2023. <https://ourworldindata.org/artificial-intelligence>.
- [7] David Patterson, Joseph Gonzalez, Quoc Le, Chen Liang, Lluis-Miquel Munguia, Daniel Rothchild, David So, Maud Texier, and Jeff Dean. Carbon emissions and large neural network training, 2021.
- [8] Romal Thoppilan, Daniel De Freitas, Jamie Hall, Noam Shazeer, Apoorv Kulshreshtha, Heng-Tze Cheng, Alicia Jin, Taylor Bos, Leslie Baker, Yu Du, YaGuang Li, Hongrae Lee, Huaixiu Steven Zheng, Amin Ghafouri, Marcelo Menegali, Yanping Huang, Maxim Krikun, Dmitry Lepikhin, James Qin, Dehao Chen, Yuanzhong Xu, Zhifeng Chen, Adam Roberts, Maarten Bosma, Vincent Zhao, Yanqi Zhou, Chung-Ching Chang, Igor Krivokon, Will Rusch, Marc Pickett, Pranesh Srinivasan, Laichee Man, Kathleen Meier-Hellstern, Meredith Ringel Morris, Tulsee Doshi, Renelito Delos Santos, Toju Duke, Johnny Soraker, Ben Zevenbergen, Vinodkumar Prabhakaran, Mark Diaz, Ben Hutchinson, Kristen Olson, Alejandra Molina, Erin Hoffman-John, Josh Lee, Lora Aroyo, Ravi Rajakumar, Alena Butryna, Matthew Lamm, Viktoriya Kuzmina, Joe Fenton, Aaron Cohen, Rachel Bernstein, Ray Kurzweil, Blaise Aguera-Arcas, Claire Cui, Marian Croak, Ed Chi, and Quoc Le. Lamda: Language models for dialog applications, 2022.
- [9] Tom B. Brown, Benjamin Mann, Nick Ryder, Melanie Subbiah, Jared Kaplan, Prafulla Dhariwal, Arvind Neelakantan, Pranav Shyam, Girish Sastry, Amanda Askell, Sandhini Agarwal, Ariel Herbert-Voss, Gretchen Krueger, Tom Henighan, Rewon Child, Aditya Ramesh, Daniel M. Ziegler, Jeffrey Wu, Clemens Winter, Christopher Hesse, Mark Chen, Eric Sigler, Mateusz Litwin, Scott Gray, Benjamin Chess, Jack Clark, Christopher Berner, Sam McCandlish, Alec Radford, Ilya Sutskever, and Dario Amodei. Language models are few-shot learners, 2020.

- [10] Zachary Champion. Optimization could cut the carbon footprint of ai training by up to 75%, April 2023.
- [11] Scott Robbins and Aimee van Wynsberghe. Our new artificial intelligence infrastructure: Becoming locked into an unsustainable future. *Sustainability*, 14(8):4829, April 2022.
- [12] Hanchen Wang, Tianfan Fu, Yuanqi Du, Wenhao Gao, Kexin Huang, Ziming Liu, Payal Chandak, Shengchao Liu, Peter Van Katwyk, Andreea Deac, Anima Anandkumar, Karianne Bergen, Carla P. Gomes, Shirley Ho, Pushmeet Kohli, Joan Lasenby, Jure Leskovec, Tie-Yan Liu, Arjun Manrai, Debora Marks, Bharath Ramsundar, Le Song, Jimeng Sun, Jian Tang, Petar Veličković, Max Welling, Linfeng Zhang, Connor W. Coley, Yoshua Bengio, and Marinka Zitnik. Scientific discovery in the age of artificial intelligence. *Nature*, 620(7972):47–60, August 2023.
- [13] Kevin Schawinski, M. Dennis Turp, and Ce Zhang. Exploring galaxy evolution with generative models. *Astronomy & Astrophysics*, 616:L16, August 2018.
- [14] Yolanda Gil, Mark Greaves, James Hendler, and Haym Hirsh. Amplify scientific discovery with artificial intelligence. *Science*, 346(6206):171–172, October 2014.
- [15] Wei-Hao Chen, Kai-Xiang Li, Wei-Yu Lin, Kuo-Hsiang Hsu, Pin-Yi Li, Cheng-Han Yang, Cheng-Xin Xue, En-Yu Yang, Yen-Kai Chen, Yun-Sheng Chang, Tzu-Hsiang Hsu, Ya-Chin King, Chorng-Jung Lin, Ren-Shuo Liu, Chih-Cheng Hsieh, Kea-Tiong Tang, and Meng-Fan Chang. A 65nm 1mb nonvolatile computing-in-memory reram macro with sub-16ns multiply-and-accumulate for binary dnn ai edge processors. In *2018 IEEE International Solid - State Circuits Conference - (ISSCC)*, pages 494–496, 2018.
- [16] Mark Horowitz. 1.1 computing's energy problem (and what we can do about it). In *2014 IEEE International Solid-State Circuits Conference Digest of Technical Papers (ISSCC)*. IEEE, February 2014.
- [17] Shantanu Chakrabartty and Gert Cauwenberghs. Performance walls in machine learning and neuromorphic systems. In *2023 IEEE International Symposium on Circuits and Systems (ISCAS)*, pages 1–4, 2023.
- [18] L. P. Shi, K. J. Yi, K. Ramanathan, R. Zhao, N. Ning, D. Ding, and T. C. Chong. Artificial cognitive memory—changing from density driven to functionality driven. *Applied Physics A*, 102(4):865–875, February 2011.
- [19] Shubham Rai, Mengyun Liu, Anteneh Gebregiorgis, Debjyoti Bhattacharjee, Krishnendu Chakrabarty, Said Hamdioui, Anupam Chattopadhyay, Jens Trommer, and Akash Kumar. Perspectives on emerging computation-in-memory paradigms. In *2021 Design, Automation & Test in Europe Conference & Exhibition (DATE)*, pages 1925–1934, 2021.
- [20] Wenqiang Zhang, Bin Gao, Jianshi Tang, Peng Yao, Shimeng Yu, Meng-Fan Chang, Hoi-Jun Yoo, He Qian, and Huaqiang Wu. Neuro-inspired computing chips. *Nature Electronics*, 3(7):371–382, July 2020.
- [21] Weier Wan, Rajkumar Kubendran, Clemens Schaefer, Sukru Burc Eryilmaz, Wenqiang Zhang, Dabin Wu, Stephen Deiss, Priyanka Raina, He Qian, Bin Gao, Siddharth Joshi, Huaqiang Wu, H.-S. Philip Wong, and Gert Cauwenberghs. A compute-in-memory chip based on resistive random-access memory. *Nature*, 608(7923):504–512, August 2022.
- [22] Shantanu Chakrabartty and Gert Cauwenberghs. Sub-microwatt analog vlsi trainable pattern classifier. *IEEE Journal of Solid-State Circuits*, 42(5):1169–1179, 2007.
- [23] Jun Yuan, Yang Zhan, William Jannen, Prashant Pandey, Amogh Akshintala, Kanchan Chandnani, Pooja Deo, Zardosht Kasheff, Leif Walsh, Michael Bender, Martin Farach-Colton, Rob Johnson, Bradley C. Kuszmaul, and Donald E. Porter. Optimizing every operation in a write-optimized file system. In *14th USENIX Conference on File and Storage Technologies (FAST 16)*, pages 1–14, Santa Clara, CA, February 2016. USENIX Association.
- [24] Philip Colangelo, Nasibeh Nasiri, Eriko Nurvitadhi, Asit Mishra, Martin Margala, and Kevin Nealis. Exploration of low numeric precision deep learning inference using intel® fpgas. In *2018 IEEE 26th Annual International Symposium on Field-Programmable Custom Computing Machines (FCCM)*, pages 73–80, 2018.
- [25] Ranjana Godse, Adam McPadden, Vipin Patel, and Jung Yoon. Memory technology enabling the next artificial intelligence revolution. In *2018 IEEE Nanotechnology Symposium (ANTS)*, pages 1–4, 2018.
- [26] Yuxin Wang, Qiang Wang, Shaohuai Shi, Xin He, Zhenheng Tang, Kaiyong Zhao, and Xiaowen Chu. Benchmarking the performance and energy efficiency of ai accelerators for ai training. In *2020 20th IEEE/ACM International Symposium on Cluster, Cloud and Internet Computing (CCGRID)*, pages 744–751, 2020.

- [27] Jiawen Liu, Hengyu Zhao, Matheus A. Ogleari, Dong Li, and Jishen Zhao. Processing-in-memory for energy-efficient neural network training: A heterogeneous approach. In *2018 51st Annual IEEE/ACM International Symposium on Microarchitecture (MICRO)*, pages 655–668, 2018.
- [28] Stefanos Georgiou, Maria Kechagia, Tushar Sharma, Federica Sarro, and Ying Zou. Green ai: Do deep learning frameworks have different costs? In *Proceedings of the 44th International Conference on Software Engineering*, pages 1082–1094, 2022.
- [29] Darshit Mehta, Mustafizur Rahman, Kenji Aono, and Shantanu Chakrabartty. An adaptive synaptic array using fowler–nordheim dynamic analog memory. *Nature Communications*, 13(1), March 2022.
- [30] Mustafizur Rahman, Subhankar Bose, and Shantanu Chakrabartty. On-device synaptic memory consolidation using fowler-nordheim quantum-tunneling. *Frontiers in Neuroscience*, 16, January 2023.
- [31] Eric R. Kandel. The molecular biology of memory storage: A dialogue between genes and synapses. *Science*, 294(5544):1030–1038, November 2001.
- [32] L. F. Abbott and Wade G. Regehr. Synaptic computation. *Nature*, 431(7010):796–803, October 2004.
- [33] Paul C. Bressloff and James N. Maclaurin. Stochastic hybrid systems in cellular neuroscience. *The Journal of Mathematical Neuroscience*, 8(1), August 2018.
- [34] Werner von Seelen and Hanspeter A. Mallot. *Parallelism and Redundancy in Neural Networks*, page 51–60. Springer Berlin Heidelberg, 1989.
- [35] Emre O. Neftci, Bruno U. Pedroni, Siddharth Joshi, Maruan Al-Shedivat, and Gert Cauwenberghs. Stochastic synapses enable efficient brain-inspired learning machines. *Frontiers in Neuroscience*, 10, June 2016.
- [36] Nuttida Rungratsameetaweemana, Robert Kim, Thiparat Chotibut, and Terrence J. Sejnowski. Random noise promotes slow heterogeneous synaptic dynamics important for robust working memory computation. *bioRxiv*, 2023.
- [37] Yandong Yin and Xin Sheng Zhao. Kinetics and dynamics of dna hybridization. *Accounts of Chemical Research*, 44(11):1172–1181, June 2011.
- [38] Charles H. Bennett. The thermodynamics of computation—a review. *International Journal of Theoretical Physics*, 21(12):905–940, December 1982.
- [39] Richard Phillips Feynman, J. G. Hey, and Robin W. Allen. *Feynman Lectures on Computation*. Addison-Wesley Longman Publishing Co., Inc., USA, 1998.
- [40] Stefano Fusi, Patrick J. Drew, and L.F. Abbott. Cascade models of synaptically stored memories. *Neuron*, 45(4):599–611, February 2005.
- [41] James Kirkpatrick, Razvan Pascanu, Neil Rabinowitz, Joel Veness, Guillaume Desjardins, Andrei A. Rusu, Kieran Milan, John Quan, Tiago Ramalho, Agnieszka Grabska-Barwinska, Demis Hassabis, Claudia Clopath, Dharshan Kumaran, and Raia Hadsell. Overcoming catastrophic forgetting in neural networks. *Proceedings of the National Academy of Sciences*, 114(13):3521–3526, March 2017.
- [42] Mary B Kennedy. Synaptic signaling in learning and memory. *Cold Spring Harb. Perspect. Biol.*, 8(2):a016824, December 2013.
- [43] C Koch and I Segev. The role of single neurons in information processing. *Nat. Neurosci.*, 3 Suppl(S11):1171–1177, November 2000.
- [44] James L McClelland, Bruce L McNaughton, and Randall C O’Reilly. Why there are complementary learning systems in the hippocampus and neocortex: insights from the successes and failures of connectionist models of learning and memory. *Psychol. Rev.*, 102(3):419–457, July 1995.
- [45] James L McClelland. Incorporating rapid neocortical learning of new schema-consistent information into complementary learning systems theory. *J. Exp. Psychol. Gen.*, 142(4):1190–1210, November 2013.
- [46] John A Swanson. Physical versus logical coupling in memory systems. *IBM Journal of Research and Development*, 4(3):305–310, 1960.
- [47] R. Landauer. Irreversibility and heat generation in the computing process. *IBM Journal of Research and Development*, 5(3):183–191, 1961.
- [48] Hiroyuki Akinaga and Hisashi Shima. Resistive random access memory (reram) based on metal oxides. *Proceedings of the IEEE*, 98(12):2237–2251, 2010.

- [49] Cheng-Xin Xue, Tsung-Yuan Huang, Je-Syu Liu, Ting-Wei Chang, Hui-Yao Kao, Jing-Hong Wang, Ta-Wei Liu, Shih-Ying Wei, Sheng-Po Huang, Wei-Chen Wei, Yi-Ren Chen, Tzu-Hsiang Hsu, Yen-Kai Chen, Yun-Chen Lo, Tai-Hsing Wen, Chung-Chuan Lo, Ren-Shuo Liu, Chih-Cheng Hsieh, Kea-Tiong Tang, and Meng-Fan Chang. 15.4 a 22nm 2mb reram compute-in-memory macro with 121-28tops/w for multibit mac computing for tiny ai edge devices. In *2020 IEEE International Solid-State Circuits Conference - (ISSCC)*, pages 244–246, 2020.
- [50] Farnood Merrikh-Bayat, Xinjie Guo, Michael Klachko, Mirko Prezioso, Konstantin K. Likharev, and Dmitri B. Strukov. High-performance mixed-signal neurocomputing with nanoscale floating-gate memory cell arrays. *IEEE Transactions on Neural Networks and Learning Systems*, 29(10):4782–4790, 2018.
- [51] S. Dünkel, M. Trentzsch, R. Richter, P. Moll, C. Fuchs, O. Gehring, M. Majer, S. Wittek, B. Müller, T. Melde, H. Mulaosmanovic, S. Slesazek, S. Müller, J. Ocker, M. Noack, D.-A. Löhr, P. Polakowski, J. Müller, T. Mikolajick, J. Höntschel, B. Rice, J. Pellerin, and S. Beyer. A fetfet based super-low-power ultra-fast embedded nvm technology for 22nm fdsoi and beyond. In *2017 IEEE International Electron Devices Meeting (IEDM)*, pages 19.7.1–19.7.4, 2017.
- [52] Tommaso Toffoli. Action, or the fungibility of computation. In *Feynman and Computation*, pages 349–392. Westview Press, 2002.
- [53] Leon Brillouin. The negentropy principle of information. *Journal of Applied Physics*, 24(9):1152–1163, 1953.
- [54] Laszlo B. Kish. Thermal noise driven computing, 2006.
- [55] Sri Harsha Kondapalli, Xuan Zhang, and Shantanu Chakrabartty. Energy-dissipation limits in variance-based computing, 2017.
- [56] Antoine Bérut, Artak Arakelyan, Artyom Petrosyan, Sergio Ciliberto, Raoul Dillenschneider, and Eric Lutz. Experimental verification of landauer’s principle linking information and thermodynamics. *Nature*, 483(7388):187–189, March 2012.
- [57] Yi-Zheng Zhen, Dario Egloff, Kavan Modi, and Oscar Dahlsten. Universal bound on energy cost of bit reset in finite time. *Physical Review Letters*, 127(19), November 2021.
- [58] Rainer Waser and Masakazu Aono. Nanoionics-based resistive switching memories. *Nature Materials*, 6(11):833–840, November 2007.
- [59] Ari Aviram. Molecules for memory, logic, and amplification. *Journal of the American Chemical Society*, 110(17):5687–5692, 1988.
- [60] Jon H Monserud and Daniel K Schwartz. Mechanisms of surface-mediated dna hybridization. *Acs Nano*, 8(5):4488–4499, 2014.
- [61] Jeremiah C Traeger and Daniel K Schwartz. Surface-mediated dna hybridization: effects of dna conformation, surface chemistry, and electrostatics. *Langmuir*, 33(44):12651–12659, 2017.
- [62] Carlo Cercignani and Carlo Cercignani. *The boltzmann equation*. Springer, 1988.
- [63] Florian Fiebig and Anders Lansner. Memory consolidation from seconds to weeks: a three-stage neural network model with autonomous reinstatement dynamics. *Frontiers in Computational Neuroscience*, 8, July 2014.
- [64] John Duchi, Elad Hazan, and Yoram Singer. Adaptive subgradient methods for online learning and stochastic optimization. *Journal of Machine Learning Research*, 12(61):2121–2159, 2011.
- [65] Diederik P. Kingma and Jimmy Ba. Adam: A method for stochastic optimization, 2014.
- [66] Leslie N. Smith and Nicholay Topin. Super-convergence: Very fast training of neural networks using large learning rates, 2017.
- [67] Youngjin Park, Woochul Choi, and Se-Bum Paik. Symmetry of learning rate in synaptic plasticity modulates formation of flexible and stable memories. *Scientific reports*, 7(1):5671, 2017.
- [68] Jack Choquette, Wishwesh Gandhi, Olivier Giroux, Nick Stam, and Ronny Krashinsky. Nvidia a100 tensor core gpu: Performance and innovation. *IEEE Micro*, 41(2):29–35, 2021.
- [69] Partha S. Chakraborty, Adilson S. Cardoso, Brian R. Wier, Anup P. Omprakash, John D. Cressler, Mehmet Kaynak, and Bernd Tillack. A 0.8 thz f_{\max} sige hbt operating at 4.3 k. *IEEE Electron Device Letters*, 35(2):151–153, 2014.

- [70] Dandan Hui, Husain Alqattan, Simin Zhang, Vladimir Pervak, Enam Chowdhury, and Mohammed Th. Hassan. Ultrafast optical switching and data encoding on synthesized light fields. *Science Advances*, 9(8):eadf1015, 2023.
- [71] Gert Cauwenberghs. Reverse engineering the cognitive brain. *Proceedings of the National Academy of Sciences*, 110(39):15512–15513, September 2013.
- [72] Rafal Karakiewicz, Roman Genov, and Gert Cauwenberghs. 1.1 tmacs/mw fine-grained stochastic resonant charge-recycling array processor. *IEEE Sensors Journal*, 12(4):785–792, 2012.
- [73] Satya N Majumdar and Grégory Schehr. Top eigenvalue of a random matrix: large deviations and third order phase transition. *Journal of Statistical Mechanics: Theory and Experiment*, 2014(1):P01012, 2014.
- [74] Ivana Đuričković, Rémy Claverie, Patrice Bourson, Mario Marchetti, Jean-Marie Chassot, and Marc D Fontana. Water–ice phase transition probed by raman spectroscopy. *Journal of Raman Spectroscopy*, 42(6):1408–1412, 2011.
- [75] Rustam Z Khaliullin, Hagai Eshet, Thomas D Kühne, Jörg Behler, and Michele Parrinello. Nucleation mechanism for the direct graphite-to-diamond phase transition. *Nature materials*, 10(9):693–697, 2011.
- [76] Rui-Hua He, M Hashimoto, H Karapetyan, JD Koralek, JP Hinton, JP Testaud, V Nathan, Y Yoshida, Hong Yao, K Tanaka, et al. From a single-band metal to a high-temperature superconductor via two thermal phase transitions. *Science*, 331(6024):1579–1583, 2011.
- [77] S. Ramprasad, N.R. Shanbhag, and I.N. Hajj. Information-theoretic bounds on average signal transition activity [vlsi systems]. *IEEE Transactions on Very Large Scale Integration (VLSI) Systems*, 7(3):359–368, 1999.
- [78] D R White, R Galleano, A Actis, H Brixy, M De Groot, J Dubbeldam, A L Reesink, F Edler, H Sakurai, R L Shepard, and J C Gallop. The status of johnson noise thermometry. *Metrologia*, 33(4):325–335, August 1996.
- [79] Elad Hazan and Satyen Kale. Beyond the regret minimization barrier: Optimal algorithms for stochastic strongly-convex optimization. *Journal of Machine Learning Research*, 15(71):2489–2512, 2014.
- [80] Marcus K Benna and Stefano Fusi. Computational principles of synaptic memory consolidation. *Nature Neuroscience*, 19(12):1697–1706, October 2016.